Defence Research and Development Canada
Recherche et développement pour la défense Canada

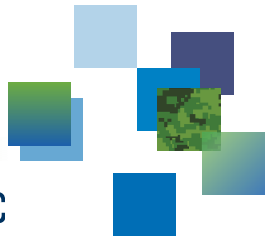

DRDC | RDDC
technologysciencetechnologie

Pattern of life model parameterization for exploitation in Command and Control systems

Methodology report part I: Target motion model and formalization

Leonardo M. Millefiori
Paolo Braca
NATO - Science & Technology Organization - Centre for Maritime Research and Experimentation

Steven Horn
DRDC – Centre for Operational Research and Analysis

Defence Research and Development Canada
Scientific Report
DRDC-RDDC-2019-R058
September 2019

Canada

IMPORTANT INFORMATIVE STATEMENTS

This document was reviewed for Controlled Goods by DRDC using the Schedule to the *Defence Production Act*.

Endorsement statement: This publication has been peer-reviewed and published by the Editorial Office of Defence Research and Development Canada, an agency of the Department of National Defence of Canada. Inquiries can be sent to: Publications.DRDC-RDDC@drdc-rddc.gc.ca.

Abstract

Extracting valuable information from large spatio-temporal datasets requires innovative approaches that can efficiently deal with large amounts of data and, at the same time, effectively reveal the underlying structure of the data, in order to provide useful information to the decision making process.

Innovative knowledge discovery techniques have been developed which use a stochastic mean-reverting modeling of the ships motion to reveal the underlying graphical structure of maritime traffic. The generated knowledge enables numerous possibilities, from graph-based multi-edge prediction to anomaly detection techniques, to ship routing optimization. Altogether, the topics covered in this report represent the theoretical framework that is required for the development of knowledge discovery techniques able to reveal the underlying graph structure of maritime traffic, which are documented in the companion report—Part II.

This report—Part I—documents the formalization of the ship motion model, motivating its use over other conventional models. Procedures to estimate the process parameters are provided and its use for long-term prediction and data association is investigated. The main limitation of this model, its applicability to non-maneuvering targets only, is also overcome by formalizing an augmented version of the model that fits the case of a vessel navigating by waypoints. Real-world data sets are used to show the potential of the developed techniques in cases of practical relevance.

This work was done within the DRDC-CMRE collaborative research activity "Pattern of life model parameterization for exploitation in Command and Control systems" under the DRDC Project 01da on Next Generation Naval Command and Control Systems.

Significance for defence and security

Understanding maritime traffic patterns is a part of a more complete Maritime Situational Awareness (MSA) and, ultimately, required to effectively classify and predict activities of ships at sea. The amount of information currently available about ships at sea is overwhelming to human operators, and the aid of automatic processing is necessary and required to *synthesize* the information in clear and effective forms that highlight important features and reject noise.

This report is a foundation for the development of a statistical framework for future knowledge discovery techniques that can derive synthetic graphical representations of the maritime traffic, which at the same time is able to efficiently handle the large amounts of data at hand.

Including a capability in next generation C2 systems to derive and represent Pattern of Life also provides more effective decision making for operational and tactical planning. For example, the more accurate predictability of maritime traffic enables practical sensor cross cuing by space-based assets. This enhances the space based ability to track and monitor vessels of interest. Another example is the consideration of pattern of life information to plan maneuvers in areas where a Navy has little prior experience. By having available the automatically derived pattern of life available in an operating area, military planners will be able to include this information to make more effective decisions either to ensure the safety of their own forces, or to apply a greater operational non-munitions effect.

Résumé

L'extraction de l'information précieuse à partir de grands ensembles de données spatio-temporelles nécessite des approches novatrices en mesure de traiter efficacement un grand volume d'information tout en révélant la structure sous-jacente des données. Elle est ainsi capable de fournir des renseignements utiles au processus décisionnel.

On a mis au point des techniques novatrices de découverte des connaissances à l'aide d'une modélisation stochastique du mouvement des navires par retour à la moyenne en vue de révéler la structure graphique sous-jacente du trafic maritime. Les connaissances générées offrent de nombreuses possibilités, allant de la prédiction multibord graphique aux techniques de détection d'anomalies, en passant par l'optimisation des routes des navires. Regroupés, les sujets abordés dans le présent rapport représentent le cadre théorique nécessaire à l'élaboration de techniques de découverte des connaissances capables de révéler la structure graphique sous-jacente du trafic maritime, qui sont documentées dans le rapport complémentaire - Partie II.

Le présent rapport, Partie I, documente la formalisation du modèle de mouvement du navire et promeut l'emploi de ce dernier plutôt que des autres modèles conventionnels. En outre, il comprend des procédures d'estimation des paramètres du processus et on y étudie l'information sur l'exécution de ce processus dans le cadre de la prévision à long terme et de l'association de données. La principale limite de ce modèle, à savoir son applicabilité à des cibles sans manoeuvres seulement, est surmontée par la formalisation d'une version améliorée adaptée au cas d'un navire naviguant à l'aide de points de cheminement. On utilise des ensembles de données en situation réelle afin de démontrer le potentiel des techniques élaborées dans des cas d'intérêt pratique.

On a réalisé ce travail dans le cadre de l'activité de recherche concertée de RDDC CREM «paramétrage du modèle du mode de vie aux fins d'exploitation dans les systèmes de commandement et de contrôle » du projet 01da de RDDC sur les systèmes de commandement et de contrôle navals de prochaine génération.

Importance pour la défense et la sécurité

Comprendre les structures du trafic maritime fait partie d'une connaissance de la situation maritime (CSM) exhaustive et, au final, est nécessaire pour classer et prédire les activités des navires en mer. Les opérateurs humains croulent sous le volume d'information actuellement disponible sur les navires en mer ; ils nécessitent donc une solution de traitement automatique, également requise en vue de synthétiser l'information sous des formes claires et concises qui soulignent les caractéristiques importantes et rejettent les données superflues.

Ce rapport sert de fondement à l'élaboration d'un cadre statistique pour les futures techniques de découverte des connaissances qui permettront d'obtenir des synthèses graphiques du trafic maritime ainsi que de traiter le volume important de données dont on dispose.

l'inclusion, dans les systèmes de C et C de prochaine génération, d'une capacité de dériver et de représenter le mode de vie améliore le processus décisionnel relatif à la planification opérationnelle et tactique. Par exemple, une prévisibilité accrue du trafic maritime permet la signalisation réciproque d'objectifs par capteurs géospatiaux. On améliore ainsi la capacité d'assurer la surveillance et le suivi spatiaux des navires d'intérêt. Un autre exemple est la prise en compte de l'information sur le mode de vie pour planifier les manœuvres dans les zones où la Marine a peu d'expérience antérieure. En disposant d'un mode de vie dérivé automatiquement dans une zone d'opération, les planificateurs militaires pourront inclure cette information afin d'améliorer la prise de décisions pour assurer la sécurité de leurs propres forces ou pour appliquer un plus grand nombre d'incidences opérationnelles sans munitions.

Table of contents

List of figures

List of tables

1 Introduction

Maritime Situational Awareness (MSA), which is the understanding of all the activities carried out in the maritime domain and surrounding environment [1], is essential in order to support a timely decision making process. A key component of MSA is the surveillance of traffic at sea. Thanks to technological advances and international regulations, a robust global surveillance capability for ships at sea is becoming a reality, even though several limitations still remain.

Maritime traffic monitoring networks are increasingly being used for global-scale surveillance. These networks are mainly based on the Automatic Identification System (AIS) with which ships, among other related information, broadcast their position, speed and course details. Coastal radar and Synthetic Aperture Radar (SAR) systems also contribute and complement the picture as non-cooperative surveillance systems, but the amount of data they produce is inevitably less than that generated by AIS networks.

Due to increasing traffic at sea and widespread compliance with national and international requirements, worldwide networks of AIS receivers have considerably grown in the last decade and are generating larger and larger volumes of AIS data. Examples of global AIS networks can be easily found documented in literature that receive 800 million AIS messages every month, broadcast by over 100 000 unique vessels all over the world, just through coastal receivers [2]. In addition to this, Satellite AIS (S-AIS) is providing detection capability for non-coastal regions, with performance that depends on satellite revisit rates, ship traffic density, and other factors [3].

Such amounts of data clearly pose significant challenges in terms of algorithmic complexity and scalability, aspects that cannot be overlooked when it comes to design and plan for any real-world application. Even more importantly, human operators cannot possibly process these volumes of data and therefore suitable algorithms are strictly required to extract information that can be useful for the decision making process. Scientists and researchers have exerted significant effort in the study and design of proper methods to extract information about ships' behaviors, patterns and statistics, effectively converting AIS, originally conceived only for collision avoidance, into an essential means to achieve useful MSA.

Global AIS coverage is now an accepted reality. However, in practice, there are still many factors negatively impacting the achievable refresh time (i.e. the frequency at which new information is received). These factors include: the ability of a vessel to turn off their AIS transponder, the higher error rate with respect to terrestrial AIS at longer range, or unfavorable weather conditions (rain fade and similar phenomena). Another reason is message collisions: the AIS protocol was designed for local radio broadcast, but when receiving S-AIS over large field of view the probability of message

collisions is significantly higher, effectively reducing the error-free detection rate.

In practice, vessels in open seas are often not *continuously* observed, and the resulting coverage gaps clearly pose a challenge for wide area tracking. The impact of this reduction in persistence would be in some sense be mitigated if accurate predictions of ships' positions could be computed as they navigate through such coverage gaps.

Unfortunately, the problem of accurate, long-term (i.e. several hours) vessel state prediction has been somewhat overlooked in the tracking literature, with only few works (partially) addressing this problem [4, 5]. In fact, the most widely adopted motion model, namely the Nearly Constant Velocity (NCV) model [6, 7] is notably not well suited to represent the long-term evolution of a vessel's motion, as the vessel position and velocity are unbounded; from another perspective, this amounts to the uncertainty of the predicted position increasing cubically with the prediction time. In conventional tracking applications, this is not a significant issue[1], but it is for long-term predictions. The use of the more suitable but less commonly used Ornstein-Uhlenbeck (OU) process to model kinematics is not completely new to the tracking community, and can be found described in a few works [9, 10, 11] available in literature. The OU model is used here, to apply a a zero-mean-reversion effect, with the aim being an improved short-term characterization of the target dynamics prior to the long-term state prediction.

A novel formulation of the long-term prediction problem has recently been proposed [8] and validated [12] against a very large dataset of AIS messages collected in the Mediterranean Sea and broadcast by commercial ships. The proposed modeling uses the OU process to stochastically represent the velocity of the vessel. With respect to the NCV model, the OU process has an additional feedback loop that ensures the velocity is bounded over time. In practice, there is a tendency of the process to revert to a defined velocity value when the process value has moved away from it; this effect is also called the mean-reversion effect. A similar process extending the OU approach has been presented in [13] which adds further constrains on the vessel movement variabilities for long-term state prediction. The simpler OU process model from [8] is used for this work.

With this model, the prediction error covariance (uncertainty of the prediction) in the position is a much more constrained time scaling law, increasing only linearly (instead of cubically) with the prediction time, thanks to the additional feedback loop. In other words, the proposed formulation reduces by orders of magnitude the prediction error covariance (uncertainty). More importantly, it has been shown that,

[1] In conventional tracking applications, the surveillance systems are usually synchronous, meaning they have a fixed scan time, and the prediction is referred to one time scan ahead [8]. The duration of the scan time depends on the specific surveillance system, but is certainly short enough not to be considered as *long-term* future.

as the prediction time increases, the motion of the majority of commercial maritime traffic is actually better modeled with the OU process than it is with the NCV.

With the same formalism as in [8], this report provides a broader sight on the global theoretical framework and presents its applicative implications of operational relevance, paving the way for the companion report—Part II that develops graph-based knowledge discovery techniques. The present report is organized as follows. First, the stochastic state equation is formalized and specialized to the OU mean-reverting velocity motion model; an optimal prediction procedure and two different Maximum Likelihood (ML) estimation techniques for the process parameters are introduced, and the applicability of the prediction technique to the problem of long-term data association is shown. Then, the focus will move onto the extension of the model from [8] to the case of ship waypoint navigation, effectively mitigating the main limitation of the modeling: its applicability to non-maneuvering vessels only. Finally, some experimental results are presented, along with future perspectives in this line of research.

2 Dynamics model

This section is devoted to the formalization of the stochastic model for the vessel dynamics. In [8], a stochastic mean-reverting process is proposed to represent the vessel velocity. We will build on the same approach, which is different from that is usually taken in conventional tracking applications, where the vessel velocity is assumed constant in time and perturbed only by a white-noise process. The immediate consequence of this formalism is that the vessel velocity grows unbounded with time. To the contrary, the mean-reversion effect is obtained with a feedback loop that maintains the vessel velocity bounded around a finite value, eventually making the model better suited for long-term state predictions. Let us now indicate the state at time $t \in \mathbb{R}_0^+$ with

$$\boldsymbol{s}(t) := [x(t),\, y(t),\, \dot{x}(t),\, \dot{y}(t)]^{\mathsf{T}}, \tag{1}$$

where the two coordinates $x(t)$ and $y(t)$, and the corresponding velocities $\dot{x}(t)$ and $\dot{y}(t)$, in a two-dimensional Cartesian (x, y) reference system[2] are also denoted by

$$\boldsymbol{x}(t) := [x(t),\, y(t)]^{\mathsf{T}} \tag{2}$$

$$\dot{\boldsymbol{x}}(t) := [\dot{x}(t),\, \dot{y}(t)]^{\mathsf{T}}. \tag{3}$$

In general, the vessel dynamics can be represented by a set of linear stochastic differential equation (SDE), in the form [6]:

$$\mathrm{d}\boldsymbol{s}(t) = \boldsymbol{A}\boldsymbol{s}(t)\,\mathrm{d}t + \boldsymbol{G}\boldsymbol{u}(t)\,\mathrm{d}t + \boldsymbol{B}\,\mathrm{d}\boldsymbol{w}(t), \tag{4}$$

where $\boldsymbol{A}$, $\boldsymbol{B}$ and $\boldsymbol{G}$ are constant matrices, $\boldsymbol{u}(t)$ is a deterministic function, and $\boldsymbol{w}(t)$ is a standard bi-dimensional Wiener process. The first-order moment of the solution of the state equation above lend itself to be interpreted, in the Bayesian sense, as the optimal prediction equation for future states. In other words, given a state $\boldsymbol{s}(t_0)$, the optimal predictor of the state at a future time $t > t_0$ can be written as follows

$$\boldsymbol{s}(t|t_0) = \mathbb{E}\left[\boldsymbol{s}(t)\,|\boldsymbol{s}(t_0)\right] := [x(t|t_0), y(t|t_0), \dot{x}(t|t_0), \dot{y}(t|t_0)]^{\mathsf{T}}, \tag{5}$$

where $\mathbb{E}[\cdot]$ denotes the expected value operator. The main advantage of using a mean-reverting process to represent the velocity component of the vessel state is related to the properties of the Bayesian predictor, especially when $t - t_0$ is not comparable to the refresh period of the sensor that generates the measurements, being instead orders of magnitude longer. Unsurprisingly, the estimator is highly dependent on the specific stochastic process used in (4).

While usually the state observation is typically assumed to be affected by noise, in our approach we assume direct observation of the vessel positional state. This

[2] The choice to define the vessel state in the Cartesian coordinates is a standard one in the tracking literature, e.g. see [7].

assumption might seem unrealistic, but it is plausible when considering some types of real-world data, such as the AIS, with which ships broadcast their Global Positioning System (GPS) position, whose measurement noise is negligible if compared with the average size of commercial ships. Moreover, the assumption does not imply a loss in generality and can be removed later.

Now, assuming that the vessel velocity can be modeled with an OU model, the SDE (4) specializes to:

$$\mathrm{d}\boldsymbol{s}(t) = \boldsymbol{A}\,\boldsymbol{s}(t)\,\mathrm{d}t + \boldsymbol{G}\,\boldsymbol{v}\,\mathrm{d}t + \boldsymbol{B}\;\mathrm{d}\boldsymbol{w}(t), \tag{6}$$

where the control input accounts for the mean-reverting tendency of the velocity, $\boldsymbol{v} = [v_x, v_y]^\mathsf{T}$, and $\boldsymbol{w}(t)$ is a standard bi-dimensional Wiener process. The matrices $\boldsymbol{A}$, $\boldsymbol{B}$ and $\boldsymbol{G}$ are defined as:

$$\boldsymbol{A} = \begin{bmatrix} \boldsymbol{0} & \boldsymbol{I} \\ \boldsymbol{0} & -\boldsymbol{\Theta} \end{bmatrix}, \quad \boldsymbol{B} = \begin{bmatrix} \boldsymbol{0} \\ \boldsymbol{C} \end{bmatrix}, \quad \boldsymbol{G} = \begin{bmatrix} \boldsymbol{0} \\ \boldsymbol{\Theta} \end{bmatrix}, \tag{7}$$

being $\boldsymbol{\Theta}$ and $\boldsymbol{C}$ generic bi-dimensional matrices. Equation (6) has the form of a Langevin dynamics [14] and can be solved in closed form by using Itô calculus [15, 16]; more details about the solution of the state equation can be found in Sect. 2.1. If the $\dot{\boldsymbol{x}}(t)$ process can be said to be of Ornstein-Uhlenbeck (OU) type [17, 18], correspondingly we can say that $\boldsymbol{x}(t)$ is an Integrated Ornstein-Uhlenbeck (IOU) process [18]. The parameters v_x and v_y in $\boldsymbol{v} = [v_x, v_y]^\mathsf{T}$ play a key role in the proposed model, as they represent the *typical* velocities along x and y, respectively, of the vessel on the trajectory under consideration. Roughly speaking, the velocity of the process tends to drift over time towards its long-term mean; and the mean-reversion tendency is stronger when the velocity is further away from that long-term mean. In our application, this "mean" velocity is the ship *cruise* or *desired* velocity.

Finally, the diagonal terms of $\boldsymbol{\Theta}$ represent the mean reversion effect along the x and y components, respectively, while the off-the-diagonal elements are representative of the coupling effect between them. In any case, if $\boldsymbol{\Theta}$ is diagonalizable and has positive eigenvalues, an affine transformation can be found that projects the matrix $\boldsymbol{\Theta}$ onto another space where the reversion rate matrix is diagonal, i.e. $\boldsymbol{\Theta} = \boldsymbol{R}\boldsymbol{\Gamma}\boldsymbol{R}^{-1}$, being $\boldsymbol{\Gamma}$ a diagonal matrix. This idea is further expanded in Sec 2.2, where the general solution to the coupled problem is provided.

2.1 Prediction procedure

As already mentioned, once that (6) is solved, the first-order moment of the solution of the SDE [15, 18] provides for the optimal state prediction $\boldsymbol{s}\,(t\,|t_0\,)$, and the second-order one for the related variance, which we will take as a measure of the prediction uncertainty. This section is devoted to the derivation of the optimal prediction procedure when the vessel velocity is represented by an OU process.

Let us now assume, in the first instance, that $\boldsymbol{\Theta} = \boldsymbol{\Gamma} = \operatorname{diag}(\boldsymbol{\gamma})$ is diagonal, being $\boldsymbol{\gamma} = [\gamma_x, \gamma_y]^\mathsf{T}$ the vector of eigenvalues of $\boldsymbol{\Theta}$ and devote Sect. 2.2 to the general solution. For a moment, we will consider the velocity and positional parts of the state separately. For the velocity part, we have that

$$\dot{\boldsymbol{x}}(t|t_0) = \boldsymbol{v} + \begin{bmatrix} \mathrm{e}^{-\gamma_x(t-t_0)} & 0 \\ 0 & \mathrm{e}^{-\gamma_y(t-t_0)} \end{bmatrix} (\dot{\boldsymbol{x}}(t_0) - \boldsymbol{v}) \,. \tag{8}$$

Proceeding similarly for the vessel position, which is an IOU process, the following expression can be derived

$$\boldsymbol{x}(t|t_0) = \boldsymbol{x}(t_0) + (t - t_0)\ \boldsymbol{v} + \begin{bmatrix} \frac{1-\mathrm{e}^{-\gamma_x(t-t_0)}}{\gamma_x} & 0 \\ 0 & \frac{1-\mathrm{e}^{-\gamma_y(t-t_0)}}{\gamma_y} \end{bmatrix} (\dot{\boldsymbol{x}}(t_0) - \boldsymbol{v}) \,. \tag{9}$$

Equations (8)–(9) can be assembled together to obtain the optimal prediction in matrix form

$$\boldsymbol{s}(t|t_0) = \boldsymbol{\Phi}(t - t_0, \boldsymbol{\gamma})\, \boldsymbol{s}(t_0) + \boldsymbol{\Psi}(t - t_0, \boldsymbol{\gamma})\, \boldsymbol{v}, \tag{10}$$

where $\boldsymbol{\Phi}(t, \boldsymbol{\gamma})$ is the analogue of the state transition matrix and $\boldsymbol{\Psi}(t, \boldsymbol{\gamma})\, \boldsymbol{v}$ is often called the control input function. Their definitions are respectively provided by equations (21) and (23) in Sect. 2.2.

Similarly, the estimator error covariance can be computed from the second moment of the SDE solution, and its full expression is provided by (26) in Sect. 2.2. The variance terms can be expressed as

$$\mathbb{E}\left[\left(x\left(t|t_0\right) - x\left(t\right) \right)^2 | \, \boldsymbol{x}(t_0) \right] = \frac{\sigma_x^2}{\gamma_x^3} f\left(\gamma_x\ (t - t_0)\right) \tag{11}$$

$$\mathbb{E}\left[\left(y\left(t|t_0\right) - y\left(t\right) \right)^2 | \, \boldsymbol{y}(t_0) \right] = \frac{\sigma_y^2}{\gamma_y^3} f\left(\gamma_y\ (t - t_0)\right) \tag{12}$$

$$\mathbb{E}\left[\left(\dot{x}\left(t|t_0\right) - \dot{x}\left(t\right) \right)^2 | \, \dot{\boldsymbol{x}}(t_0) \right] = \frac{\sigma_x^2}{\gamma_x} g\left(\gamma_x\ (t - t_0)\right) \tag{13}$$

$$\mathbb{E}\left[\left(\dot{y}\left(t|t_0\right) - \dot{y}\left(t\right) \right)^2 | \, \dot{\boldsymbol{y}}(t_0) \right] = \frac{\sigma_y^2}{\gamma_y} g\left(\gamma_y\ (t - t_0)\right), \tag{14}$$

where σ_x^2 and σ_y^2 are the diagonal elements of $\boldsymbol{C}\boldsymbol{C}^\mathsf{T}$, and $f(t)$ and $g(t)$ are the prediction position and velocity error as *normalized* variance and are defined as

$$f\left(t\right) := \frac{1}{2}\left(2t + 4\mathrm{e}^{-t} - \mathrm{e}^{-2t} - 3\right) \tag{15}$$

$$g\left(t\right) := \frac{1}{2}\left(1 - \mathrm{e}^{-2t}\right). \tag{16}$$

2.2 Coupled Ornstein-Uhlenbeck process

Let us now remove the assumption of $\boldsymbol{\Theta}$ being a diagonal matrix. We will show that the optimal predictor shares the same basic structure of (10). To this aim, we shall consider the SDE (6) again; by Itô calculus [16, 19], the first two moments are computable as follows

$$\mathbb{E}\left[\boldsymbol{s}(t)\,|\boldsymbol{s}(t_0)\right] = \mathrm{e}^{\boldsymbol{A}(t-t_0)}\boldsymbol{s}(t_0) + \int_{t_0}^{t} \mathrm{e}^{\boldsymbol{A}(t-s)}\boldsymbol{G}\,\boldsymbol{v}\,\mathrm{d}s, \tag{17}$$

and

$$\mathbb{C}\left[\boldsymbol{s}(t)\,|\boldsymbol{s}(t_0)\right] = \int_{t_0}^{t} \mathrm{e}^{\boldsymbol{A}(t-s)}\boldsymbol{B}\boldsymbol{B}^{\mathsf{T}}\left(\mathrm{e}^{\boldsymbol{A}(t-s)}\right)^{\mathsf{T}}\mathrm{d}s, \tag{18}$$

being $\mathbb{C}[\cdot]$ the covariance operator. Assuming that $\boldsymbol{\Theta}$ is diagonalizable, i.e. $\boldsymbol{\Theta} = \boldsymbol{R}\boldsymbol{\Gamma}\boldsymbol{R}^{-1}$ represents its eigen decomposition, then the following relations hold

$$\boldsymbol{A} = \begin{bmatrix} \boldsymbol{0} & \boldsymbol{I} \\ \boldsymbol{0} & -\boldsymbol{\Theta} \end{bmatrix} = \begin{bmatrix} \boldsymbol{0} & \boldsymbol{I} \\ \boldsymbol{0} & -\boldsymbol{R}\boldsymbol{\Gamma}\boldsymbol{R}^{-1} \end{bmatrix} = \widetilde{\boldsymbol{R}}\widetilde{\boldsymbol{A}}\widetilde{\boldsymbol{R}}^{-1},$$

where

$$\widetilde{\boldsymbol{R}} := \begin{bmatrix} \boldsymbol{R} & \boldsymbol{0} \\ \boldsymbol{0} & \boldsymbol{R} \end{bmatrix} \quad \text{and} \quad \widetilde{\boldsymbol{A}} := \begin{bmatrix} \boldsymbol{0} & \boldsymbol{I} \\ \boldsymbol{0} & -\boldsymbol{\Gamma} \end{bmatrix}. \tag{19}$$

We can now exploit the power series of the matrix exponential to obtain a convenient expression for $\mathrm{e}^{\boldsymbol{A}t}$

$$\begin{aligned} \mathrm{e}^{\boldsymbol{A}t} &= \sum_{k=0}^{\infty} \frac{1}{k!}\,\boldsymbol{A}^k t^k \\ &= \sum_{k=0}^{\infty} \frac{1}{k!} \prod_{i=0}^{k} \left(\widetilde{\boldsymbol{R}}\,\widetilde{\boldsymbol{A}}\widetilde{\boldsymbol{R}}^{-1}\right) t^k \\ &= \sum_{k=0}^{\infty} \frac{1}{k!}\,\widetilde{\boldsymbol{R}}\,\widetilde{\boldsymbol{A}}^k t^k \widetilde{\boldsymbol{R}}^{-1} \\ &= \widetilde{\boldsymbol{R}}\left(\sum_{k=0}^{\infty} \frac{1}{k!}\,\widetilde{\boldsymbol{A}}^k t^k\right)\widetilde{\boldsymbol{R}}^{-1} \\ &= \widetilde{\boldsymbol{R}}\,\mathrm{e}^{\widetilde{\boldsymbol{A}}t}\,\widetilde{\boldsymbol{R}}^{-1}, \end{aligned} \tag{20}$$

that can be reworked to highlight the dependence on t and $\boldsymbol{\gamma}$

$$\boldsymbol{\Phi}\left(t, \boldsymbol{\gamma}\right) := \mathrm{e}^{\widetilde{\boldsymbol{A}}t} = \begin{bmatrix} \boldsymbol{I} & \left(\boldsymbol{I} - \mathrm{e}^{-\boldsymbol{\Gamma}\,t}\right)\boldsymbol{\Gamma}^{-1} \\ \boldsymbol{0} & \mathrm{e}^{-\boldsymbol{\Gamma}\,t} \end{bmatrix}. \tag{21}$$

On the other hand, the integral in (17) can be written in terms of $\boldsymbol{\Phi}\left(t, \boldsymbol{\gamma}\right)$

$$\boldsymbol{\Psi}(t, \boldsymbol{\gamma}) := \int_{t_0}^{t} \mathrm{e}^{\boldsymbol{A}(t-s)}\,\boldsymbol{G}\;\mathrm{d}s = \int_{t_0}^{t} \boldsymbol{\Phi}\left(t-s, \boldsymbol{\gamma}\right)\begin{bmatrix} \boldsymbol{0} \\ \boldsymbol{\Gamma} \end{bmatrix}\mathrm{d}s, \tag{22}$$

and allows for a closed-form solution

$$\boldsymbol{\Psi}(t,\boldsymbol{\gamma}) = \begin{bmatrix} t\,\boldsymbol{I} - \left(\boldsymbol{I} - \mathrm{e}^{-\boldsymbol{\Gamma}\,t}\right)\boldsymbol{\Gamma}^{-1} \\ \boldsymbol{I} - \mathrm{e}^{-\boldsymbol{\Gamma}\,t} \end{bmatrix}. \tag{23}$$

Combining together (17), (21) and (23) leads us to the first moment of the SDE solution, which indeed shares the same structure of (10), apart from the projection operated by $\widetilde{\boldsymbol{R}}$, i.e.

$$\boldsymbol{s}(t|t_0) = \widetilde{\boldsymbol{R}}\boldsymbol{\Phi}\left(t-t_0,\boldsymbol{\gamma}\right)\widetilde{\boldsymbol{R}}^{-1}\boldsymbol{s}(t_0) + \widetilde{\boldsymbol{R}}\,\boldsymbol{\Psi}\left(t-t_0,\boldsymbol{\gamma}\right)\boldsymbol{R}^{-1}\boldsymbol{v}, \tag{24}$$

where $\boldsymbol{\Phi}\left(t,\boldsymbol{\gamma}\right)$ is the state transition matrix and $\boldsymbol{\Psi}(t,\boldsymbol{\gamma})$ is the control input function, defined as before.

We can proceed analogously with the second order solution using eq. (18) and (21)

$$\mathbb{C}\left[\boldsymbol{s}(t)\,|\boldsymbol{s}(t_0)\right] = \widetilde{\boldsymbol{R}}\left(\int_{t_0}^{t}\boldsymbol{\Phi}\left(t-s,\boldsymbol{\gamma}\right)\begin{bmatrix}\boldsymbol{0} & \boldsymbol{0}\\ \boldsymbol{0} & \widetilde{\boldsymbol{C}}\end{bmatrix}\boldsymbol{\Phi}^{T}\left(t-s,\boldsymbol{\gamma}\right)\mathrm{d}s\right)\widetilde{\boldsymbol{R}}^{-1} \tag{25}$$

where $\widetilde{\boldsymbol{C}}$ is the noise covariance in the *transformed* domain, whose entries are defined as follows

$$\widetilde{\boldsymbol{C}} := \boldsymbol{R}^{-1}\boldsymbol{C}\left(\boldsymbol{R}^{-1}\boldsymbol{C}\right)^{\mathsf{T}} = \begin{bmatrix}\sigma_x^2 & \sigma_{xy}\\ \sigma_{xy} & \sigma_y^2\end{bmatrix}.$$

Again, the problem can be solved in algebraically closed-form and for the second moment of the SDE solution, we obtain

$$\mathbb{C}\left[\boldsymbol{s}(t)\,|\boldsymbol{s}(t_0)\right] = \widetilde{\boldsymbol{R}}\,\boldsymbol{\Sigma}\left(t-t_0\right)\,\widetilde{\boldsymbol{R}}^{-1}, \tag{26}$$

where $\boldsymbol{\Sigma}\left(t\right) = \boldsymbol{\Sigma}_1 \circ \boldsymbol{\Sigma}_2\left(t\right)$. The matrix $\boldsymbol{\Sigma}_1$ has the following form

$$\boldsymbol{\Sigma}_1 = \begin{bmatrix} \frac{\sigma_x^2}{\gamma_x^3} & \frac{\sigma_{xy}}{\gamma_x\gamma_y} & \frac{\sigma_x^2}{2\gamma_x^2} & \frac{2\sigma_{xy}}{\gamma_x} \\ \frac{\sigma_{xy}}{\gamma_x\gamma_y} & \frac{\sigma_y^2}{\gamma_y^3} & \frac{2\sigma_{xy}}{\gamma_y} & \frac{\sigma_y^2}{2\gamma_y^2} \\ \frac{\sigma_x^2}{2\gamma_x^2} & \frac{2\sigma_{xy}}{\gamma_y} & \frac{\sigma_x^2}{\gamma_x} & \frac{2\sigma_{xy}}{\gamma_x+\gamma_y} \\ \frac{2\sigma_{xy}}{\gamma_x} & \frac{\sigma_y^2}{2\gamma_y^2} & \frac{2\sigma_{xy}}{\gamma_x+\gamma_y} & \frac{\sigma_y^2}{\gamma_y} \end{bmatrix} \tag{27}$$

and $\boldsymbol{\Sigma}_2\left(t\right)$ is defined as follows

$$\boldsymbol{\Sigma}_2\left(t\right) = \begin{bmatrix} f(t\gamma_x) & h(t,\boldsymbol{\gamma}) & k(t\gamma_x) & \frac{g(\gamma_y\frac{t}{2})}{\gamma_y} - \frac{g((\gamma_x+\gamma_y)\frac{t}{2})}{\gamma_x+\gamma_y} \\ h(t,\boldsymbol{\gamma}) & f(t\gamma_y) & \frac{g(\gamma_x\frac{t}{2})}{\gamma_x} - \frac{g((\gamma_x+\gamma_y)\frac{t}{2})}{\gamma_x+\gamma_y} & k(t\gamma_y) \\ k(t\gamma_x) & \frac{g(\gamma_x\frac{t}{2})}{\gamma_x} - \frac{g((\gamma_x+\gamma_y)\frac{t}{2})}{\gamma_x+\gamma_y} & g(t\gamma_x) & g((\gamma_x+\gamma_y)\frac{t}{2}) \\ \frac{g(\gamma_y\frac{t}{2})}{\gamma_y} - \frac{g((\gamma_x+\gamma_y)\frac{t}{2})}{\gamma_x+\gamma_y} & k(t\gamma_y) & g((\gamma_x+\gamma_y)\frac{t}{2}) & g(t\gamma_y) \end{bmatrix}. \tag{28}$$

This latter equation is finally completed by the following function definitions of $h(t, \boldsymbol{\gamma})$ and $k(t)$, noting that $f(t)$, $g(t)$ have already been defined in (15) and (16).

$$h(t, \boldsymbol{\gamma}) := t - \frac{1 - \mathrm{e}^{-t\gamma_x}}{\gamma_x} - \frac{1 - \mathrm{e}^{-t\gamma_y}}{\gamma_y} + \frac{1 - \mathrm{e}^{-t(\gamma_x + \gamma_y)}}{\gamma_x + \gamma_y}, \tag{30}$$

$$k(t) := \mathrm{e}^{-2t} \left(1 - \mathrm{e}^{t}\right)^2. \tag{31}$$

3 Parameter estimation

At this point, the reader will notice that the optimal prediction (24) depends not only on the prediction time, but also on the long-run mean velocity $\boldsymbol{v}$ and the reversion rate $\boldsymbol{\gamma}$, the latter through the matrices $\boldsymbol{\Phi}$ and $\boldsymbol{\Psi}$. Similarly, the prediction error covariance (26) depends on these process parameters and also on the process noise $\boldsymbol{C}$. Since the parameters of the stochastic process are not known a priori in any real application, they need to be estimated. In this section, we derive a procedure to estimate the parameters $\boldsymbol{\theta} = (\boldsymbol{\theta}_x, \boldsymbol{\theta}_y)$ of the process, with

$$\boldsymbol{\theta}_x = (\sigma_x, \gamma_x, v_x) \quad \text{and} \quad \boldsymbol{\theta}_y = (\sigma_y, \gamma_y, v_y)\,. \tag{32}$$

An OU process is said to be Gaussian if, for all $t_1 < t_2 < \cdots < t_n$, the n-vector $[\boldsymbol{s}(t_1), \boldsymbol{s}(t_2), \ldots, \boldsymbol{s}(t_n)]$ is multivariate normally distributed. The OU process defined by (6) is stationary, Gaussian and Markovian and it is an example of a Gaussian process with bounded variance and stationary probability distribution, as opposed as the Wiener process. This is due to the fact that in the latter, the drift term is constant whereas in the OU it is dependent on the current value of the process: if it is less than the long-term mean, the drift will be positive; on the contrary, if the current value is higher than the long-term mean, the drift will be negative. The Gaussian OU mean-reverting process is well suited for ML methods, but Least Squares (LS) regression techniques are also applicable for the estimation of the parameters of the discrete autoregressive version of the problem. The main advantage of using the ML estimator in place of a LS technique, is that the former enables the estimation of the parameters also in the case that the observation time intervals are not uniform, which is of interest for real-world applications, where the time instants of observation are often asynchronous. In the remainder of this section we will focus exclusively on ML estimation.

The estimation will be performed by considering separately the x and y components of the kinematic state. Therefore, to simplify the notation, we will use hereafter $\boldsymbol{\theta}_{x,y}$, $\sigma_{x,y}$, $\gamma_{x,y}$ and $v_{x,y}$ to denote quantities that can equally refer to the x *or* the y coordinate.

The procedures in this section work in a batch fashion, and have for objective the estimation of $\boldsymbol{\theta}$ for a given trajectory, assuming first that either only the set of velocities is observed, and then that the entire sequence of kinematic states is observed, which are denoted by $\dot{\boldsymbol{x}}(t_j)$ and $\boldsymbol{s}(t_j)$, respectively, for $j = 1, \ldots, n$, where n is the number of samples in the trajectory.

The parameters $\boldsymbol{\theta} = (\boldsymbol{\theta}_x, \boldsymbol{\theta}_y)$ are not only unknown, but also specific to each given trajectory and have therefore to be estimated from the measurement set. Due to the

Markovian and Gaussian properties of (6) [16, 20], in the first case where only the vessel velocity is observed, the likelihood function is explicitly given by [20]

$$\mathcal{L}(\boldsymbol{\theta}) = \prod_{j=1}^{n} \phi_{\dot{\boldsymbol{x}}}\left(\dot{\boldsymbol{x}}(t_j) \,|\dot{\boldsymbol{x}}(t_{j-1}), \boldsymbol{\theta}\right), \tag{33}$$

where $\phi_{\dot{\boldsymbol{x}}}(\cdot)$ is the bivariate Gaussian distribution; while in the second case where the vessel position and velocity are both observed, the likelihood takes the form

$$\mathcal{L}(\boldsymbol{\theta}) = \prod_{j=1}^{n} \phi_{\boldsymbol{s}}\left(\boldsymbol{s}(t_j) \,|\boldsymbol{s}(t_{j-1}), \boldsymbol{\theta}\right), \tag{34}$$

where $\phi_{\boldsymbol{s}}(\cdot)$ is now a four-variate Gaussian distribution. The parameter estimate, in a ML sense, is then provided by the estimator

$$\hat{\boldsymbol{\theta}} = \arg\max_{\boldsymbol{\theta}} \mathcal{L}(\boldsymbol{\theta}).$$

However, this maximization might be computationally unfeasible. In order to simplify the estimation procedure from a computational perspective, we can instead use the marginal likelihood along x and y coordinates. This marginalization procedure is quite standard, especially from the Bayesian perspective (assuming non-informative prior in our case), i.e. the other coordinate (y if we are estimating parameters along x and vice versa) is considered a nuisance parameter. The marginal likelihoods, for the case of velocity observations only, are then given by:

$$\mathcal{L}_x(\boldsymbol{\theta}_x) = \prod_{j=1}^{n} \phi_{\dot{x}}\left(\dot{x}(t_j) \,|\dot{x}(t_{j-1}), \boldsymbol{\theta}_x\right), \tag{35}$$

$$\mathcal{L}_y(\boldsymbol{\theta}_y) = \prod_{j=1}^{n} \phi_{\dot{y}}\left(\dot{y}(t_j) \,|\dot{y}(t_{j-1}), \boldsymbol{\theta}_y\right), \tag{36}$$

where $\phi_{\dot{x}}(\cdot)$ and $\phi_{\dot{y}}(\cdot)$ are Gaussian distributions with mean and variance respectively given by the velocity components, along the corresponding coordinate, of the first-order (10) and second-order (26) moments of the solution of the SDE.

In the case the entire kinematic state is observed, the equations (35)–(36) become

$$\mathcal{L}_x(\boldsymbol{\theta}_x) = \prod_{j=1}^{n} \phi_{\boldsymbol{s}_x}\left(\boldsymbol{s}_x(t_j) \,|\dot{x}(t_{j-1}), \boldsymbol{\theta}_x\right), \tag{37}$$

$$\mathcal{L}_y(\boldsymbol{\theta}_y) = \prod_{j=1}^{n} \phi_{\boldsymbol{s}_y}\left(\boldsymbol{s}_y(t_j) \,|\dot{y}(t_{j-1}), \boldsymbol{\theta}_y\right), \tag{38}$$

where $\boldsymbol{s}_x(t) := [x(t), \dot{x}(t)]^{\mathsf{T}}$, $\boldsymbol{s}_y(t) := [y(t), \dot{y}(t)]^{\mathsf{T}}$. In this case, $\phi_{\dot{x}}(\cdot)$ and $\phi_{\dot{y}}(\cdot)$ are bivariate Gaussian distributions, whose mean and variance are given by the position

and velocity components, along one or the other coordinate, of the first-order (10) and second-order moments (26) of the solution of the SDE. Finally, the ML estimators along x and y for the given trajectory are given by

$$\begin{aligned}\hat{\boldsymbol{\theta}}_x &= \arg\max_{\boldsymbol{\theta}_x} \mathcal{L}_x\left(\boldsymbol{\theta}_x\right), \\ \hat{\boldsymbol{\theta}}_y &= \arg\max_{\boldsymbol{\theta}_y} \mathcal{L}_y\left(\boldsymbol{\theta}_y\right).\end{aligned} \tag{39}$$

3.1 Procedure

For clarity, we define a generic coordinate $u = \{x, y\}$ and a generic velocity $\dot{u} = \{\dot{x}, \dot{y}\}$, along with its corresponding long-term mean velocity $v = v_{x,y}$, reversion rate $\gamma = \gamma_{x,y}$ and noise term $\sigma = \sigma_{x,y}$. Also, when not otherwise stated, from now on the subscripts are used to indicate the time variable, i.e. $u_j = u\left(t_j\right)$, for $j = 1, \ldots, n$, where n is the number of observed states within a given trajectory.

3.1.1 ML estimation from velocity samples

Inspired by [21], in order to derive a ML procedure for the estimation of the process parameters, let us consider a single vessel trajectory, representing a realization of the OU process. We observe the sequence of velocity samples of a quasi-rectilinear vessel trajectory along a generic coordinate. Let this set be

$$\mathcal{Z} = \{\dot{u}_j\}_{j=1}^{n}.$$

In Section 3 the generic form of the likelihood of the observation, given the observations $\mathcal{Z}$ have been already provided (33) as well as a specialization for the two Cartesian components of the vessel velocity (35) and (36). Under the assumptions of stationarity, Gaussianity and Markovianity of the OU process, the log-likelihood of $\mathcal{Z}$ can be derived from (35) or (36) with the relevant components of (10) and (26). Omitting the constant terms, the log-likelihood has the form

$$\begin{aligned}\ell\left(\boldsymbol{\theta}\right) = &-\frac{n}{2}\log\left(\frac{\sigma^2}{2\gamma}\right) - \frac{1}{2}\sum_{j=1}^{n}\log\left[1 - \mathrm{e}^{-2\gamma\Delta_j}\right] \\ &- \frac{\gamma}{\sigma^2}\sum_{j=1}^{n}\frac{\left(\dot{u}_j - v - \left(\dot{u}_{j-1} - v\right)\mathrm{e}^{-\gamma\Delta_j}\right)^2}{1 - \mathrm{e}^{-2\gamma\Delta_j}}\end{aligned} \tag{40}$$

where n is the cardinality of the time intervals in $\mathcal{Z}$ and $\boldsymbol{\theta} = (v, \gamma, \sigma)$ is the set of process parameters. The term $\Delta_j = t_j - t_{j-1}$ represents the time elapsed between the j-th and the immediately previous observation, enabling eventually the possibility of estimating also the parameters of asynchronous OU processes ($\Delta_j \neq \Delta_k$, $j \neq k$).

The ML estimate $\hat{\boldsymbol{\theta}} = (\hat{v}, \hat{\gamma}, \hat{\sigma})$ given $\mathcal{Z}$ is the one that satisfies the following first order conditions

$$\left.\frac{\partial \ell(\boldsymbol{\theta})}{\partial v}\right|_{\hat{v}} = 0, \quad \left.\frac{\partial \ell(\boldsymbol{\theta})}{\partial \gamma}\right|_{\hat{\gamma}} = 0, \quad \left.\frac{\partial \ell(\boldsymbol{\theta})}{\partial \sigma}\right|_{\hat{\sigma}} = 0. \tag{41}$$

The log-likelihood (40) can be elaborated and leads us to the marginal likelihood of $\mathcal{Z}$ with respect to v

$$\frac{\partial \ell(\boldsymbol{\theta})}{\partial v} = -\frac{\gamma}{\sigma^2} \sum_{j=1}^{n} \frac{\dot{u}_j - v - (\dot{u}_{j-1} - v)\, \mathrm{e}^{-\gamma \Delta_j}}{1 + \mathrm{e}^{-\gamma \Delta_j}}. \tag{42}$$

Assuming γ and σ are non-zero, the first order conditions (41) leads to the ML estimate of the long-term mean of the process:

$$\hat{v} = f(\hat{\gamma}) = \sum_{j=1}^{n} \frac{\dot{u}_j - \dot{u}_{j-1}\, \mathrm{e}^{-\hat{\gamma} \Delta_j}}{1 + \mathrm{e}^{-\hat{\gamma} \Delta_j}} \left(\sum_{j=1}^{n} \frac{1 - \mathrm{e}^{\hat{\gamma} \Delta_j}}{1 + \mathrm{e}^{\hat{\gamma} \Delta_j}} \right)^{-1}. \tag{43}$$

From here, following the same approach as before, one can differentiate (40) with respect to σ, thus obtaining the marginal log-likelihood of $\mathcal{Z}$

$$\frac{\partial \ell(\boldsymbol{\theta})}{\partial \sigma} = -\frac{n}{\sigma} + \frac{2\gamma}{\sigma^3} \sum_{j=1}^{n} \frac{\left(\dot{u}_j - v - (\dot{u}_{j-1} - v)\, \mathrm{e}^{-\gamma \Delta_j}\right)^2}{1 - \mathrm{e}^{-2\gamma \Delta_j}}, \tag{44}$$

which, if combined with conditions (41), provides an estimate of the noise term σ

$$\hat{\sigma} = g(\hat{v}, \hat{\gamma}) = \sqrt{\frac{2\hat{\gamma}}{n} \sum_{j=1}^{n} \frac{\left(\dot{u}_j - \hat{v} - (\dot{u}_{j-1} - \hat{v})\, \mathrm{e}^{-\hat{\gamma} \Delta_j}\right)^2}{1 - \mathrm{e}^{-2\hat{\gamma} \Delta_j}}}.$$

The system of non-linear equations given by $\hat{v} = f(\hat{\gamma})$ and $\hat{\sigma} = g(\hat{v}, \hat{\gamma})$ together with conditions (41) would lead to the ML estimator of γ, but the solution would not be available in closed form. A different approach is to substitute $\hat{v} = f(\hat{\gamma})$ and $\hat{\sigma} = g(\hat{v}, \hat{\gamma})$ directly into the likelihood function (40), obtaining the following

$$\begin{aligned} V(\gamma) = &-\frac{n}{2} \log \left(\frac{g(f(\gamma)), \gamma)^2}{2\gamma} \right) \\ &- \frac{1}{2} \sum_{j=1}^{n} \log \left(1 - \mathrm{e}^{-2\gamma \Delta_j}\right) \\ &- \frac{\gamma}{\tilde{g}_\gamma^2} \sum_{j=1}^{n} \frac{\left(\dot{u}_j - f(\gamma) - (\dot{u}_j - f(\gamma))\, \mathrm{e}^{-\gamma \Delta_j}\right)^2}{1 - \mathrm{e}^{-2\gamma \Delta_j}}, \end{aligned} \tag{45}$$

having defined $\tilde{g}_\gamma = g\left(f\left(\gamma\right), \gamma\right)$. Contrary to the solution of the aforementioned system of non-linear equations, the minimization of (45) is a one-dimensional search problem, whose solution can be shown to be the ML estimator of γ:

$$\hat{\gamma} = \arg\min_{\gamma} V\left(\gamma\right).$$

3.1.2 ML estimation from position and velocity samples

In the previous section, a procedure to compute the ML estimate of the process parameters has been described that only uses the velocity part of the state. With a similar approach, we also derive another ML estimation procedure, which now processes also the positional part of the state. Let us consider the joint position-velocity state along a generic coordinate $\boldsymbol{u}_i = [u(t_i), \dot{u}(t_i)]^\mathsf{T}$ and let the set of observations be

$$\mathcal{Z} = \{\boldsymbol{u}_j\}_{j=1}^n.$$

Under the same hypotheses as in Sect. 3.1.1, the likelihood of $\mathcal{Z}$ along one of the Cartesian coordinate and with respect to the process parameters γ and σ, given the long-run mean parameter v, is provided by the specialization of (37)– (38), i.e.

$$\mathcal{L}(\gamma, \sigma) = \prod_{j=1}^{n} \frac{|\boldsymbol{\Sigma}_i(\gamma)|^{-\frac{1}{2}}}{2\pi\sigma^2} \mathrm{e}^{-\frac{\lambda_i(\gamma)}{2\sigma^2}}, \tag{46}$$

with

$$\lambda_i(\gamma) := \boldsymbol{\mu}_i^\mathsf{T} \boldsymbol{\Sigma}_i^{-1}(\gamma) \boldsymbol{\mu}_i \tag{47}$$

and $\boldsymbol{\mu}_i$ is the difference between the state at time t_i and the state predicted after Δ_i seconds from $\boldsymbol{u}_{i-1}$:

$$\boldsymbol{\mu}_i := \boldsymbol{u}_i - \boldsymbol{\Phi}(\gamma, \Delta_i)\boldsymbol{u}_{i-1} - \boldsymbol{\Psi}(\gamma, \Delta_i)\, v. \tag{48}$$

The matrices $\boldsymbol{\Phi}$ and $\boldsymbol{\Psi}$ are the single-coordinate versions of (21) and (23), respectively. Analogously, $\boldsymbol{\Sigma}_i$ is the single-coordinate version of (26), i.e.

$$\boldsymbol{\Sigma}_i\left(\gamma\right) := \sigma^2 \begin{bmatrix} 1/\gamma^3 & 1/2\gamma^2 \\ 1/2\gamma^2 & 1/\gamma \end{bmatrix} \circ \begin{bmatrix} f(\gamma, \Delta_i) & k(\gamma, \Delta_i) \\ k(\gamma, \Delta_i) & g(\gamma, \Delta_i) \end{bmatrix}, \tag{49}$$

where f, g and k are defined in (15), (16) and (31), respectively. Finally, the log-likelihood can be written as

$$\ell(\gamma, \sigma) = -n\left(\log\sigma^2 + \log 2\pi\right) - \frac{1}{2}\sum_{j=1}^{n}\left(\log|\boldsymbol{\Sigma}_i(\gamma)| + \frac{\lambda_i\left(\boldsymbol{\gamma}\right)}{\sigma^2}\right). \tag{50}$$

Proceeding as before, one can marginalize the log-likelihood 50 as follows

$$\left.\frac{\partial\,\ell\,(\gamma,\sigma)}{\partial\sigma^2}\right|_{\hat{\sigma}} = 0 \Rightarrow \hat{\sigma}(\gamma) = \sqrt{\frac{1}{2n}\sum_{i=1}^{n}\lambda_i(\gamma)}, \tag{51}$$

in order to obtain a functional form for the ML estimate of σ that depends only on γ, which can be inserted back into (50) to remove the dependency on σ. Finally, the ML estimate of γ amounts to a one-dimensional maximization operation, i.e.

$$\hat{\gamma} = \arg\max_{\gamma} \ell(\gamma, \hat{\sigma}(\gamma)). \tag{52}$$

At this point the reader will note that this second ML procedure only provides for the γ and σ parameter estimates, but not for the long-run mean velocity v. Indeed, in this approach this parameter has to be estimated first, for instance with a Sample Mean Estimator (SME), which has been shown [22] to be consistent when the observation sampling time is random, asymptotically efficient when the sampling time is constant, and very close to the Cramér-Rao Lower Bound (CRLB) in cases of practical interest for MSA, with a performance that can be quantified analytically in closed form.

4 Long-term data association

The proposed ship motion modeling is relevant to several applications of operational relevance, such as the association of contacts from multiple sensors that are highly intermittent or not synchronized. An example of this situation is the combined use of SAR and (especially satellite) AIS observations, which are collected when the satellite passes over the vessel, and made available when the satellite passes over a downlink station. This can easily result in a several hours time difference between the observation of the scene by the SAR and AIS sensors. It is therefore crucial to accurately compute a vessel's position from the time instant of one acquisition to the time instant of the other, and it is especially important in trafficked areas, as an accurate prediction procedure might be the only way to achieve the unambiguous association of detections.

Another situation for the application of the OU modeling is the capability to accurately estimate the future evolution of a vessel's motion in the long term, under normal circumstances, in order, for instance, to acquire the vessel with other sensors that might have to be tasked or deployed in advance. Being able to accurately predict the region of probable presence of the vessel in the long-term future increases the sensor scheduling time horizon and, in turn, enables an overall more efficient allocation of assets.

We refer to this class of problems as long-term prediction and association problems, which is discussed in this section. We leverage the OU model to formalize a simple yet effective gating procedure to associate heterogeneous observations of the same vessel taken in different times, such as AIS and SAR data, even when the time difference is of several hours. A metric is introduced to assess the performance of the association procedure with respect to a baseline reference represented by the NCV motion model. The experimental results obtained with the tools presented in this section are left to Section 6.

4.1 Data gating strategy

The procedure to associate AIS contacts with their counterpart detections in a SAR image is as simple as to propagate the vessel kinematic state at the time of the SAR image acquisition, given the past AIS observations. To do so, a multidimensional gating procedure can be used between the kinematic state predicted with the AIS (and its error covariance) and the SAR data. A measurement in the gate, while not guaranteed to have originated from the vessel the gate pertains to, is a valid association candidate. Hence, the name of *validation region* or *association region*.

We assume that the SAR data $\boldsymbol{\delta}_k$ at frame k coming from a vessel t (i.e. a vessel detected in an image acquired by a SAR system) is Gaussian distributed with mean

$\hat{\boldsymbol{x}}^t_{k|k-1}$ and covariance $\mathbf{P}^t_{k|k-1}$. Thus, its gate $\mathcal{V}^{t,\gamma}_k$ at frame k is defined by

$$\mathcal{V}^{t,\gamma}_k = \left\{ \boldsymbol{\delta} : \left[\boldsymbol{\delta} - \hat{\boldsymbol{x}}^t_{k|k-1}\right]^{\mathrm{T}} \left(\mathbf{P}^t_{k|k-1}\right)^{-1} \left[\boldsymbol{\delta} - \hat{\boldsymbol{x}}^t_{k|k-1}\right] \leq \gamma \right\}, \tag{53}$$

with a probability depending on the threshold γ. The distance metric in (53) is also called the Mahalanobis distance, which is a multi-dimensional generalization of the idea of measuring how many standard deviations away a point $\boldsymbol{\delta}$ is from the mean $\hat{\boldsymbol{x}}^t_{k|k-1}$ of the related Gaussian distribution. Under the above-mentioned hypothesis, this quadratic form is chi-squared distributed with n_x degrees of freedom, n_x being the dimension of the positional part of the state. Thus, the probability P_G that $\boldsymbol{\delta}_k$ is in $\mathcal{V}^{t,\gamma}_k$ is defined as $P\left\{\boldsymbol{\delta}_k \in \mathcal{V}^{t,\gamma}_k\right\}$, which depends on both n_x and γ [7]. Finally, it is worth remarking that the square root g of the threshold γ, i.e. $g = \sqrt{\gamma}$, is often referred to as "number of sigmas" (standard deviations) of the gate.

Remark: $\hat{\boldsymbol{x}}^t_{k|k-1}$ and $\mathbf{P}^t_{k|k-1}$ are given by the prediction formulas in Section 2.1. The model parameters are estimated from the acquired AIS data in batches by exploiting the procedure described in Section 3.

The gate equation (53) itself is a good starting point in order to define a suitable metric to assess the performance of the gating procedure. This performance metric, that we call the Gate Volume (GV) is, in other words, a measurement of how large the gate is and, by extension, how *ambiguous* the association is. The GV can be defined as the volume $V^{t,\gamma}_k$ of the gating region $\mathcal{V}^{t,\gamma}_k$ in (53) corresponding to the threshold $\gamma = g^2$ for vessel t at frame k. The GV is the volume of the confidence region from a multivariate normal distribution. The equation is [23]:

$$V^{t,\gamma}_k = c_{n_x} \left|\gamma \mathbf{P}^t_{k|k-1}\right|^{1/2} = c_{n_x} g^{n_x} \left|\mathbf{P}^t_{k|k-1}\right|^{1/2}, \tag{54}$$

where $|\cdot|$ indicates the determinant,

$$c_{n_x} = \frac{\pi^{n_x/2}}{\Gamma\left(n_x/2 + 1\right)}, \tag{55}$$

and $\Gamma(\cdot)$ is the Gamma function. Assuming the NCV as a baseline reference, in Section 6.2 we will show, in a real-world application, how the GV reflects the capability of the OU modeling to significantly reduce the potential association ambiguity.

5 A model for waypoint navigation

The majority of the maritime traffic is very regular, which can be observed in Figure 1, where a ship traffic density map is shown. Maritime vessels, and especially commercial vessels, generally seek to minimize fuel consumption and will therefore navigate along the shortest path allowed by international and regional regulations.

Several works can be found in the pertaining scientific literature that, inspired by the overall regularity of the maritime traffic, propose knowledge discovery algorithms and strategies to extract synthetic representations of the maritime traffic [4, 5]. This report shares that same basic intuition and overarching ambition. However, unlike previous work, the fundamental building block here is the OU model. The main limitation of this model which must be overcome is the validity only for non-maneuvering vessels, meaning until the long-run mean velocity is constant[3].

A modelling approach is inspired by the traffic behavior observed in Figure 1, where evidently a significant part of the maritime traffic proceeds from waypoint to way-

[3] More precisely, the modeling is valid until *any* of the process parameters does not change in time. However, in our experience the effect of a change in the reversion rate or process noise can be considered *prima facie* a second order effect.

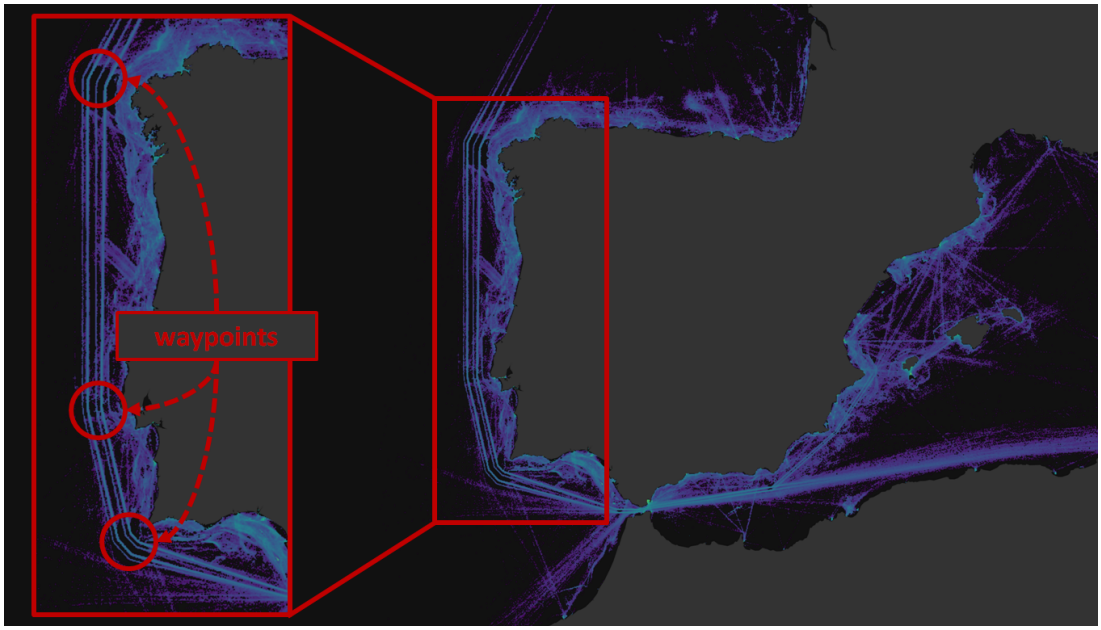

Figure 1: *Maritime traffic density off the coast of Portugal. Higher concentrations of traffic appear more green, and low concentrations as purple. It is apparent how maritime traffic follows straight paths, or* legs *between consecutive waypoints. The waypoint regions are also very localized in space.*

point, with very linear paths (legs) connecting the waypoints one to the other. Consequently, a natural extension of the OU is that of waypoint navigation, where the long-run mean velocity $\boldsymbol{v}$ is a piecewise function of time that is constant when the ship is on a navigational leg, and has abrupt changes at waypoints and stopping points. In this way, the state is still described by (6), with the only difference that the long-run mean velocity $\boldsymbol{v}$ is a piecewise-constant function of the time, defined as

$$\boldsymbol{v}(t) := \begin{cases} \boldsymbol{v}_1 & \text{for} & & & t & \leq & t^{*(1)} \\ \boldsymbol{v}_2 & \text{for} & t^{*(1)} & < & t & \leq & t^{*(2)} \\ \vdots & & & & \vdots & & \\ \boldsymbol{v}_n & \text{for} & t^{*(n-1)} & < & t & \leq & t^{*(n)} \\ \boldsymbol{v}_{n+1} & \text{for} & t^{*(n)} & < & t, & & \end{cases} \tag{56}$$

where $t^{*(i)}$ is the time of the i-th waypoint, which correspond to a change of the long-run mean velocity from the regime before to the one after the waypoint.

5.1 Change detection: single waypoint with known parameters

Following the theoretical framework formulation of quickest change detection [24], a statistical procedure can be put in place to automatically estimate the long-run mean velocity parameters on the navigational legs, detect the abrupt changes, and then identify time and location of the changes.

Let us start the formulation with a simple case of detecting a single waypoint. It is assumed that at an unknown time instant t^* the long-run mean velocity abruptly changes from $\boldsymbol{v}_0$ (hypothesis $\mathcal{H}_0$) to $\boldsymbol{v}_1$ (hypothesis $\mathcal{H}_1$), and the position of the waypoint (stopping point) is given by $\boldsymbol{x}^c = \boldsymbol{x}(t^*)$. The difference between a waypoint and a stopping point is easily understood: the former is a change from, and to, a non-zero velocity, i.e. $\boldsymbol{v}_0 \neq \boldsymbol{0}$ and $\boldsymbol{v}_1 \neq \boldsymbol{0}$, while the latter point is a point where the vessel stops, i.e. $\boldsymbol{v}_1 = \boldsymbol{0}$.

We assume that the time change t^* is synchronized with observation time instants, i.e. $t^* = t_{k^*} \in \{t_k\}_{k=1}^n$. Let us also elaborate the difference between two consecutive instantaneous velocity samples of the vessel as follows

$$\boldsymbol{z}_k = \dot{\boldsymbol{x}}_k - \boldsymbol{J}_k \dot{\boldsymbol{x}}_{k-1}, \quad \text{with} \quad \boldsymbol{J}_k := \boldsymbol{R} \mathrm{e}^{-\boldsymbol{\Gamma} t} \boldsymbol{R}^{-1}, \tag{57}$$

recalling that $\boldsymbol{R}$ is the matrix of eigenvectors of $\boldsymbol{\Theta}$ and $\boldsymbol{\Gamma} := \mathrm{diag}(\boldsymbol{\gamma})$. In this way, the $\boldsymbol{z}_k$ are time independent Gaussian random variables, i.e.

$$\boldsymbol{z}_k \sim \mathcal{N}\left(\boldsymbol{z}; \left(\boldsymbol{I} - \boldsymbol{J}_k\right) \boldsymbol{v}; \boldsymbol{\Xi}_k\right)$$

with $\boldsymbol{v} \in \{\boldsymbol{v}_0, \boldsymbol{v}_1\}$. In our notation, $\mathcal{N}\left(\boldsymbol{z}; \boldsymbol{\mu}; \boldsymbol{\Xi}\right)$ denotes a Gaussian Probability Density Function (PDF) with mean $\boldsymbol{\mu}$ and covariance $\boldsymbol{\Xi}$. The mean of each $\boldsymbol{z}_k$ is dependent

on the long-term velocity, therefore the waypoint (stopping point) can be found by detecting a change in the mean of $\boldsymbol{z}_k$.

Formally, in this case study, we have, $\forall k$:

$$\begin{aligned} f_0(\boldsymbol{z}_k) &: \boldsymbol{z}_1, \boldsymbol{z}_2, \ldots, \boldsymbol{z}_{k^*-1} \\ & \qquad\qquad \searrow \\ f_1(\boldsymbol{z}_k) &: \qquad\qquad\qquad \boldsymbol{z}_{k^*}, \boldsymbol{z}_{k^*+1}, \ldots \end{aligned} \tag{58}$$

where $f_{0,1}(\boldsymbol{z}_k) = \mathcal{N}\left((\boldsymbol{I} - \boldsymbol{J}_k)\,\boldsymbol{v}_{0,1}; \boldsymbol{\Xi}_k\right)$.

Now, in the case that all the parameters are known, i.e. the $f_{0,1}(\boldsymbol{z}_k)$ are perfectly known, the most suitable change detection procedure is Page's test [25], as it has asymptotically optimal properties (further details in [24]). Page's test is based on the clipped Cumulative Sum (CUSUM) statistic:

$$S_k = \max\left\{0, S_{k-1} + \log\frac{f_1(\boldsymbol{z}_k)}{f_0(\boldsymbol{z}_k)}\right\}, \quad S_0 = 0. \tag{59}$$

In practice, a change from $\boldsymbol{v}_0$ to $\boldsymbol{v}_1$ is declared when S_k exceeds a threshold h, and such stopping time can be defined as

$$\mathcal{K} = \min\left\{k : S_k > h\right\}. \tag{60}$$

In the change detection framework the performance is defined in terms of Average Run Length (ARL), under both hypotheses $\mathcal{H}_{0,1}$ [24]. Specifically, the ARL under $\mathcal{H}_1$ is the expected detection delay, i.e. the expected number of samples to wait for correctly detecting a change; while the ARL under $\mathcal{H}_0$ is the expected number of samples for observing an erroneous detection (false alarm).

The time of the change can be estimated with a ML procedure [24] that looks for the time of the last CUSUM reset before the stopping time. As in [24], we have, for our case:

$$\begin{aligned} \hat{k}^* &= \mathcal{K} - N_{\mathcal{K}} + 1, \\ N_k &= N_{k-1}\mathbf{1}_{\{S_{k-1}>0\}} + 1. \end{aligned} \tag{61}$$

Where $N_{\mathcal{K}}$ is the number of observations since the last CUSUM reset. Then, the estimated time of the change is the next available $t_{\hat{k}^*}$, which is $\leq t_{\mathcal{K}}$.

5.2 Change detection: multiple waypoints with unknown parameters

In a real-world case, trajectories may contain a number of waypoints and stopping points. In other words, the the long-term velocity is a piecewise-constant function of

elements $\boldsymbol{v}_j$, $j = 0, 1, \ldots, J-1$ where J is the unknown number of all the changes. Formally, the $\boldsymbol{z}_k$ are distributed as expressed in (62), which generalizes the formulation given in (58), where $f_j(\boldsymbol{z}_k) = \mathcal{N}\left((\boldsymbol{I} - \boldsymbol{J}_k)\,\boldsymbol{v}_j; \boldsymbol{\Xi}_k\right)$.

$$
\begin{array}{lccccccc}
f_0(\boldsymbol{z}_k): & \boldsymbol{z}_1, \boldsymbol{z}_2, \cdots, \boldsymbol{z}_{k_0^*-1} & \searrow & & & & & \\
f_1(\boldsymbol{z}_k): & & & \boldsymbol{z}_{k_0^*}, \boldsymbol{z}_{k_0^*+1}, \cdots \boldsymbol{z}_{k_1^*-1} & \searrow & & & \\
f_2(\boldsymbol{z}_k): & & & & & \boldsymbol{z}_{k_1^*}, \boldsymbol{z}_{k_1^*+1}, \cdots \boldsymbol{z}_{k_2^*-1} & \searrow & \\
\vdots & & & & & & \cdots & \\
f_j(\boldsymbol{z}_k): & & & & & & \boldsymbol{z}_{k_{j-1}^*}, \boldsymbol{z}_{k_{j-1}^*+1}, \cdots \boldsymbol{z}_{k_j^*-1} & \searrow \\
\vdots & & & & & & & \cdots
\end{array}
\tag{62}
$$

Moreover, the value of each $\boldsymbol{v}_j$ is also unknown, except for the stopping points, in which the velocity after or before the change is null. To estimate the piecewise long-run mean velocity function, we propose a sequential procedure that generalizes Page's test (59). This procedure is determined by:

i) the long-run mean velocity value, $\boldsymbol{v}_j$;

ii) the changing times $t_{k_j^*}$; and

iii) the locations of the changes $\boldsymbol{x}_{k_j^*}$.

The long-run velocity can be efficiently estimated using a SME [22], provided that the underlying unknown long-run velocity value is constant. Following [24], we exploit change detection algorithms to check this assumption, assuming that the time duration between successive jumps is bounded from below. This assumption is necessary for the initial estimation of the long-run velocity to be used in the subsequent detection of change. An alternative choice to Page's test (59)-(60) is the Generalized Likelihood Ratio (GLR) test in which the null hypothesis (assumed known) is compared against an alternative hypothesis in which the parameter is unknown. Even if the GLR approach would be feasible, it is much more computationally expensive w.r.t. the proposed approach and therefore not considered here.

The joint use of the estimation in [22] and the change detection results in the following steps in the algorithm, which is also illustrated in Figure 2:

S0 Initialization. Set $j = 0$. Estimate the long-run velocity, in a fixed-size time interval N, during which the detection algorithm does not operate. The first piece of the long-run velocity function is provided by

$$\hat{\boldsymbol{v}}_0 = \frac{1}{N} \sum_{n=1}^{N} \boldsymbol{x}_n. \tag{63}$$

In the case of a waypoint, define a set of P alternative hypotheses with P long-term velocities that are relatively close to $\hat{\boldsymbol{v}}_0$, and formally indicated by $\hat{\boldsymbol{v}}_{1,p}(\delta)$, $p = 1, 2, \ldots, P$. In the case of a stopping point, the alternative hypothesis is given by a long-run velocity that is zero, then $P = 1$.

S1 Activation of the change detection algorithm to find the j-th change against one of the P alternative hypotheses. Set $S_{j,p,i} = 0$ with $i = \max\left\{\hat{k}^*_{j-1} + M, 0\right\} + N$, where $\hat{k}^*_{-1} = 0$, M is a delay parameter. Compute in parallel the following CUSUM

$$S_{j,p,k} = \max\left\{0, S_{j,p,k-1} + \log\frac{f_{j+1,p}(\boldsymbol{z}_k)}{f_j(\boldsymbol{z}_k)}\right\}, \tag{64}$$

$$\mathcal{K}_j = \min\left\{k : S_{j,p,k} > h,\ i < k \leq K\right\}, \tag{65}$$

$$p^*_j = \left\{p : S_{j,p,\mathcal{K}_j} > h\right\}, \tag{66}$$

where $f_j(\boldsymbol{z}_k)$ and $f_{j+1,p}(\boldsymbol{z}_k)$ are Gaussian distribution with long-term velocities $\hat{\boldsymbol{v}}_j$ and $\hat{\boldsymbol{v}}_{j+1,p}$, respectively, i.e. $f_0(\boldsymbol{z}_k) = \mathcal{N}\left((\boldsymbol{I} - \boldsymbol{J}_k)\,\hat{\boldsymbol{v}}_0; \boldsymbol{\Xi}_k\right)$ and $f_{j+1,p}(\boldsymbol{z}_k) = \mathcal{N}\left((\boldsymbol{I} - \boldsymbol{J}_k)\,\hat{\boldsymbol{v}}_{j+1,p}; \boldsymbol{\Xi}_k\right)$. In the case of a stopping point, $f_{j+1}(\boldsymbol{z}_k) = \mathcal{N}\left(\boldsymbol{0}; \boldsymbol{\Xi}_k\right)$. K is the number of time steps in the data.

S2 If the minimum in (65) is never reached for any p, the procedure ends.

S3 When a change is detected, the time of change is estimated as in (61):

$$\hat{k}^*_j = \mathcal{K}_j - N_{j,\mathcal{K}_j} + 1, \tag{67}$$

$$N_{j,k} = N_{j,k-1}\mathbf{1}_{\left\{S_{j,p^*_j,k-1} > 0\right\}} + 1. \tag{68}$$

The position of the change (i.e. the position of the waypoint or stopping point) is then provided by $\hat{\boldsymbol{x}}^c_j = \boldsymbol{x}(\hat{t}_{\hat{k}^*_j})$. Increment j.

S4 Update the estimation of the long-run velocity after the change has been detected:

$$\hat{\boldsymbol{v}}_j = \frac{1}{N}\sum_{n=\hat{k}^*_{j-1}+M}^{k^*_{j-1}+M+N} \boldsymbol{x}_n, \tag{69}$$

where the delay parameter M is used to skip the transitory points of the OU process that would deteriorate the estimation performance. In the case of a waypoint, the long-run velocities of the alternative hypothesis are updated accordingly to the parameters δ, otherwise the long-run velocity is null. Return to **S1**.

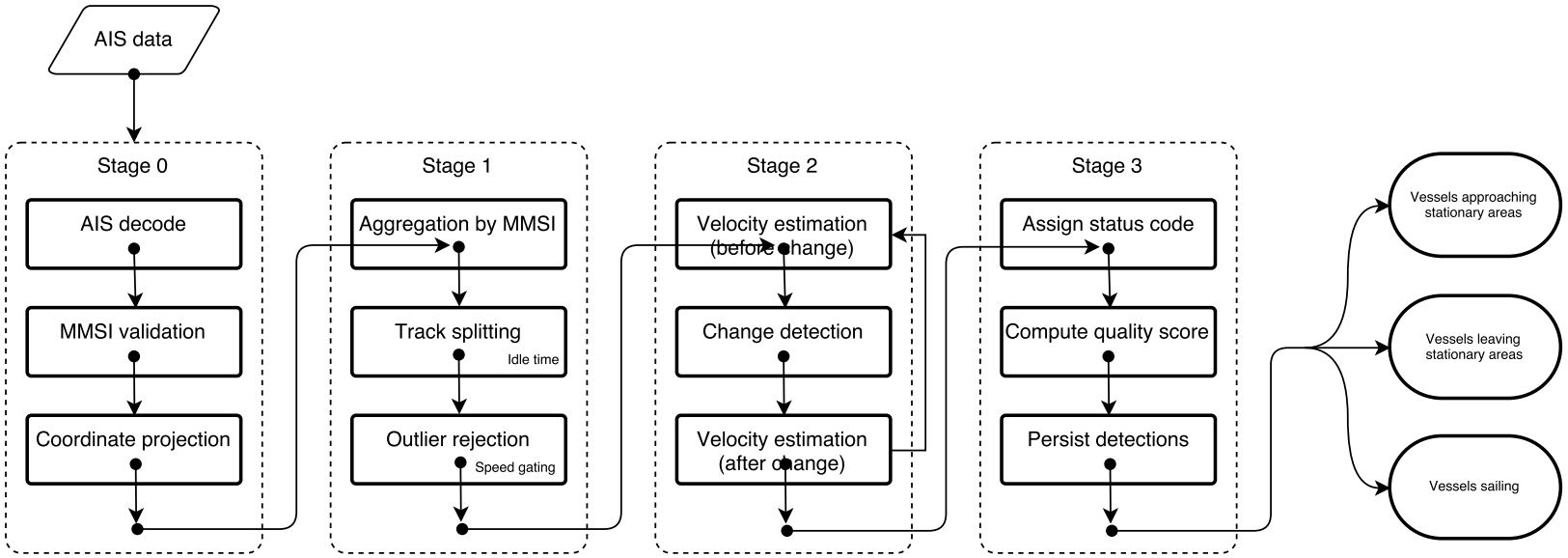

Figure 2: *Diagram of the complete change detection pipeline. The input is represented by raw AIS messages in NMEA 0183 format, that can be loaded in an Apache Spark Resilient Distributed Dataset (RDD) and immediately decoded. The blocks in Stage* 0 *and Stage* 1 *mostly deal with the pre-processing of the data set: messages with invalid Maritime Mobile Service Identifier (MMSI) numbers are discarded, the geographic coordinates are projected using the Universal Transverse Mercator (UTM) projection. In Stage* 1*, the messages are arranged first in ship tracks and then split in time-continuous segments. Outliers are rejected using a speed gating and stage* 2 *is devoted to the change detection procedure. In Stage* 3 *a status label is assigned to each detection, a quality score computed, and the Spark DataFrame of detections eventually persisted to non-volatile memory (database or file).*

For the waypoints, the alternative hypotheses should be representative of the deviations, quantified by the parameter δ, from the null hypothesis. If a bigger deviation occurs, the change will still be detected but at the cost of a degraded detection performance; in other words, the smaller is δ, the larger will be the detection delay for a given false alarm rate.

Put differently, the choice of δ poses a trade-off between the change detection performance and the capability to detect small deviations from the null hypothesis. We propose the following strategies to construct meaningful deviations from the null hypothesis:

i) two-side additive deviation on both the axes

$$\hat{\boldsymbol{v}}_{j+1,p}(\delta) = \begin{cases} \hat{\boldsymbol{v}}_j + \delta\, \boldsymbol{e}_x & p = 1 \\ \hat{\boldsymbol{v}}_j - \delta\, \boldsymbol{e}_x & p = 2 \\ \hat{\boldsymbol{v}}_j + \delta\, \boldsymbol{e}_y & p = 3 \\ \hat{\boldsymbol{v}}_j - \delta\, \boldsymbol{e}_y & p = 4 \end{cases} \tag{70}$$

where $\boldsymbol{e}_x = [1, 0]^{\mathsf{T}}$ and $\boldsymbol{e}_y = [0, 1]^{\mathsf{T}}$.

ii) two-side additive deviation on the direction $\angle\hat{\boldsymbol{v}}_j$ of the long-run velocity of the null hypothesis:

$$\|\hat{\boldsymbol{v}}_{j+1,p}(\delta)\| = \|\hat{\boldsymbol{v}}_j\|\,, \quad \angle\hat{\boldsymbol{v}}_{j+1,p}(\delta) = \begin{cases} \angle\hat{\boldsymbol{v}}_j + \delta & p = 1 \\ \angle\hat{\boldsymbol{v}}_j - \delta & p = 2 \end{cases} \tag{71}$$

Interestingly, in several real-world data sets investigated so far, we have consistently observed that vessels tend to conserve the magnitude of their velocity across the waypoints, changing only their bearing. Basically, even when maneuvering, vessels tend to preserve their momentum, which is a very reasonable behavior from the perspective of fuel consumption optimization. In this scenario, the alternative hypothesis proposed in (71) seems best suited for the problem.

A peculiar aspect of the change detection approach that has been described is that, as it is formulated, it lends itself to be implemented in a parallel and distributed fashion, such as that shown in Figure 2 and documented in [26], which leverages the Apache Spark framework.

6 Experimental Results

This section presents some typical use cases that motivated the development of the framework described in the previous sections. Towards this aim, two unclassified data sets have been used: a first one was made available by the Royal Canadian Navy (RCN) to DRDC, consisting in a large collection of ship contacts (mainly from AIS) in the North Atlantic Ocean off the coast of Canada; the second one is made up of a SAR image acquired by ESA's Sentinel-1A on the 31st of May, 2016 off the coast of Madagascar, and by the S-AIS data collected the same day in the same region that was available in CMRE's historical AIS database [2].

6.1 Canada data set: long-term association (AIS)

We have applied the OU modeling to a data set of AIS messages collected in the North Atlantic Ocean off the coast of Canada and the United States by both terrestrial and satellite AIS receivers.

Some selected trajectories, shown in Figures 3–6, have been isolated from the data set and intentionally down-sampled, in order to obtain very sparse sequences of observations of the vessels that, after this stage, detections are separated in time by several hours. Then, the first sample of each track is taken as initial state for the long-term prediction and the predicted kinematic state is computed at each time instant when an observation is made available in order to have a ground truth reference. In all the experiments, the parameters of the OU process have been estimated directly from the down-sampled data using the procedure described in Section 3.1.2, with the long-run mean velocity v estimated by the use of a SME [22]. The estimated values of the process parameters are reported in Table 1, for each presented case.

In each of the Figures 3–6, it is apparent the OU ship motion modeling is stable for long-term state prediction (and association). In all of the examples, the prediction (red crosses in the images) is qualitatively close to the ground truth (black triangles) at the time of the prediction, and the covariance ellipses are never unreasonably large (on the order of 10 to 20 km), even after the longest prediction time, 72 hours, shown in the top panel of Figure 5. In other words, the long-term prediction procedure documented in this report, is shown able to predict future positions of a vessel in the long term. This is a crucial capability requirement in order to accurately and efficiently cue, plan, and task additional reconnaissance of the vessel.

6.2 Madagascar data set: long-term association (SAR and AIS)

The second use case focuses on an example of association of AIS data with SAR detections from an image taken several hours after the ship broadcast its last position.

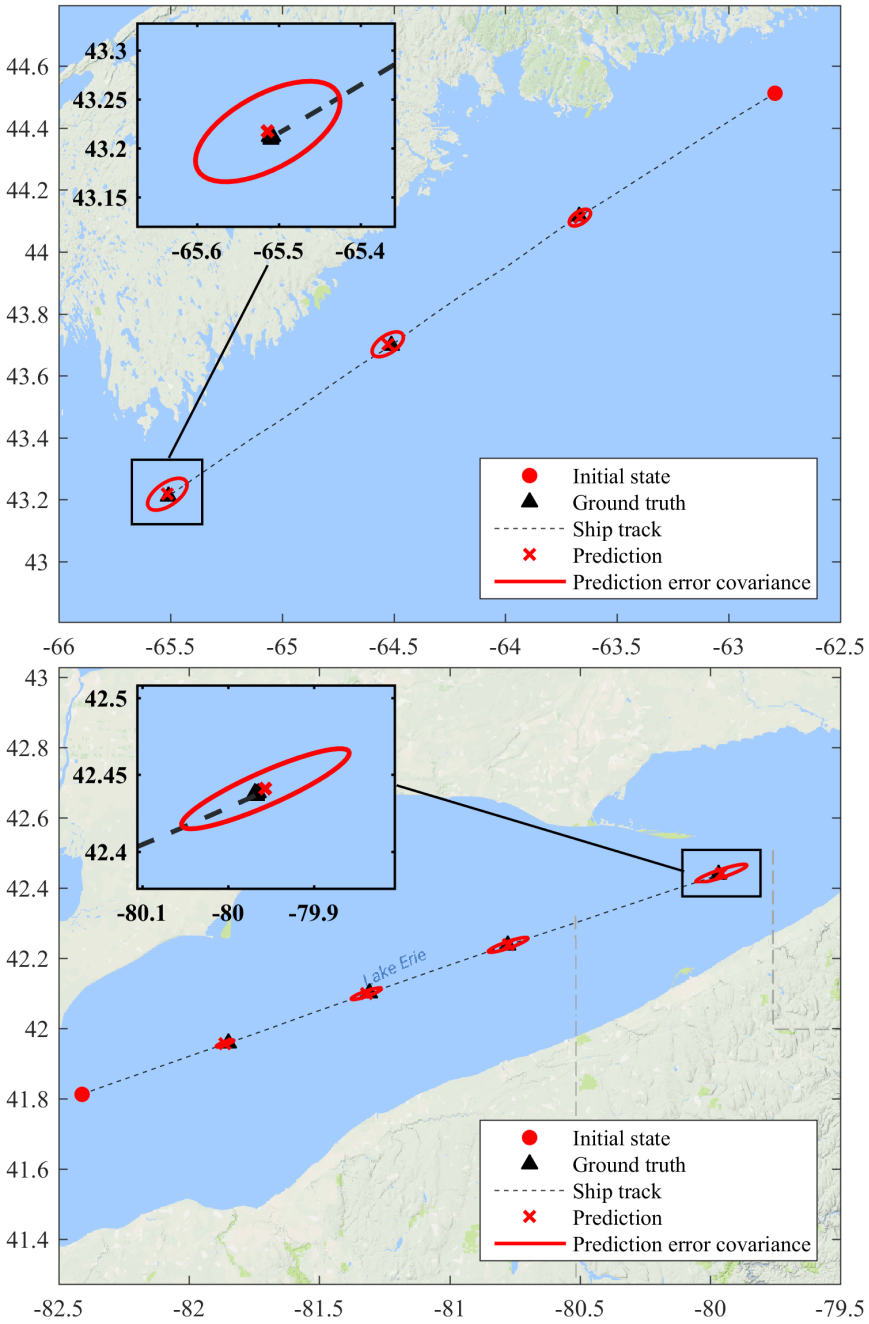

Figure 3: *Long-term association example with the proposed approach. Horizontal axis: longitude; vertical axis: latitude. Top panel: the "Acadian" oil/chemical tanker (MMSI* 316012950*) off the coast of Nova Scotia and the related position and error covariance after* 3, 6 *and* 9.5 *hours from the initial state. Bottom panel: the "Arneborg" cargo vessel (MMSI* 246556000*) in Lake Erie, with predictions at* 2, 4, 6 *and* 9 *hours after the initial state.*

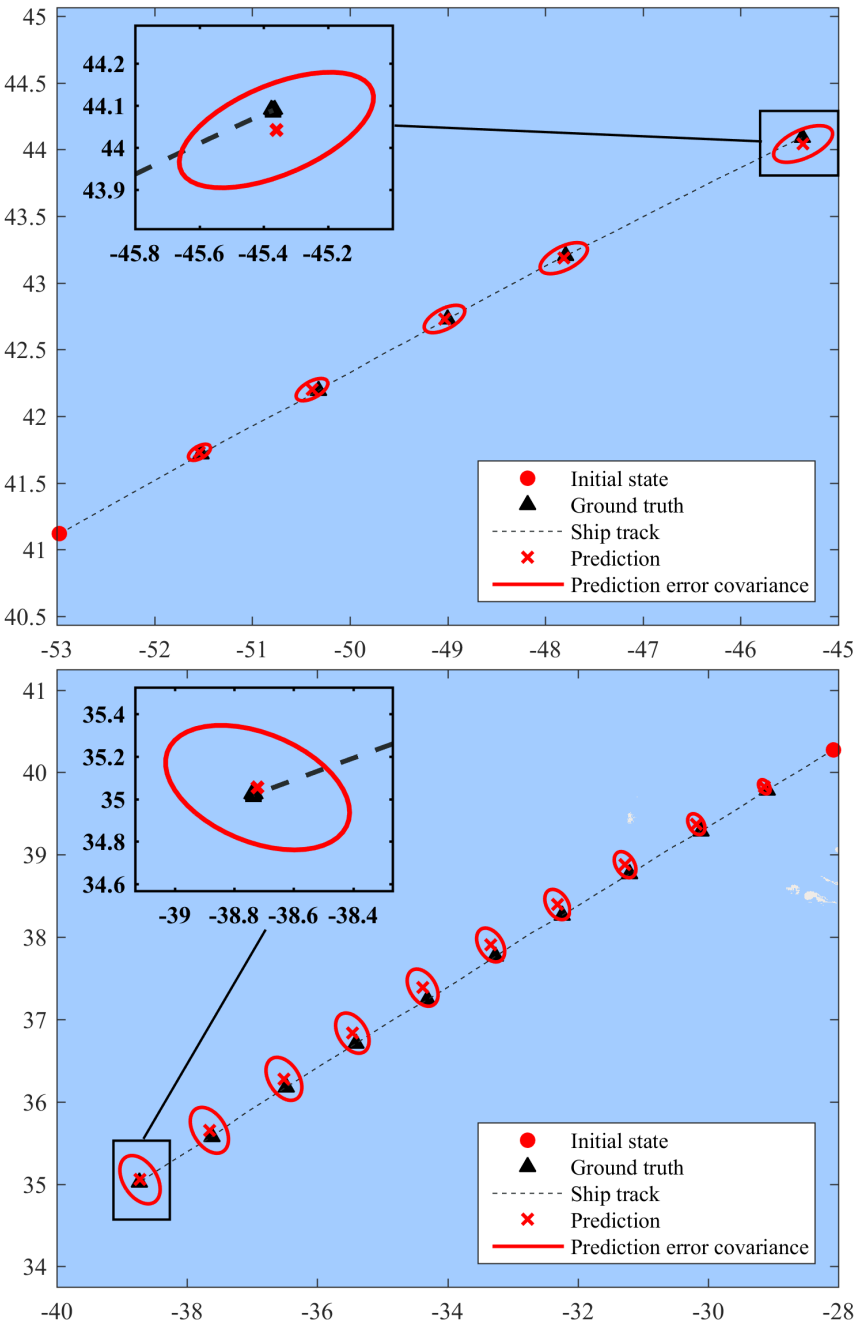

Figure 4: *Long-term association example with the proposed approach. Horizontal axis: longitude; vertical axis: latitude. Top panel: the "Niledutch Panther" container vessel (MMSI* 636017641*) in the North Atlantic Ocean and the related position and error covariance after* ≈ 4, 7, 10, 14 *and* 20 *hours from the initial state. Bottom panel: the "Nysted Maersk" cargo vessel (MMSI* 219954000*) in the North Atlantic Ocean, with predictions at every* ≈ 3 *hours after the initial state. The last prediction is* ≈ 33 *hours after the initial state.*

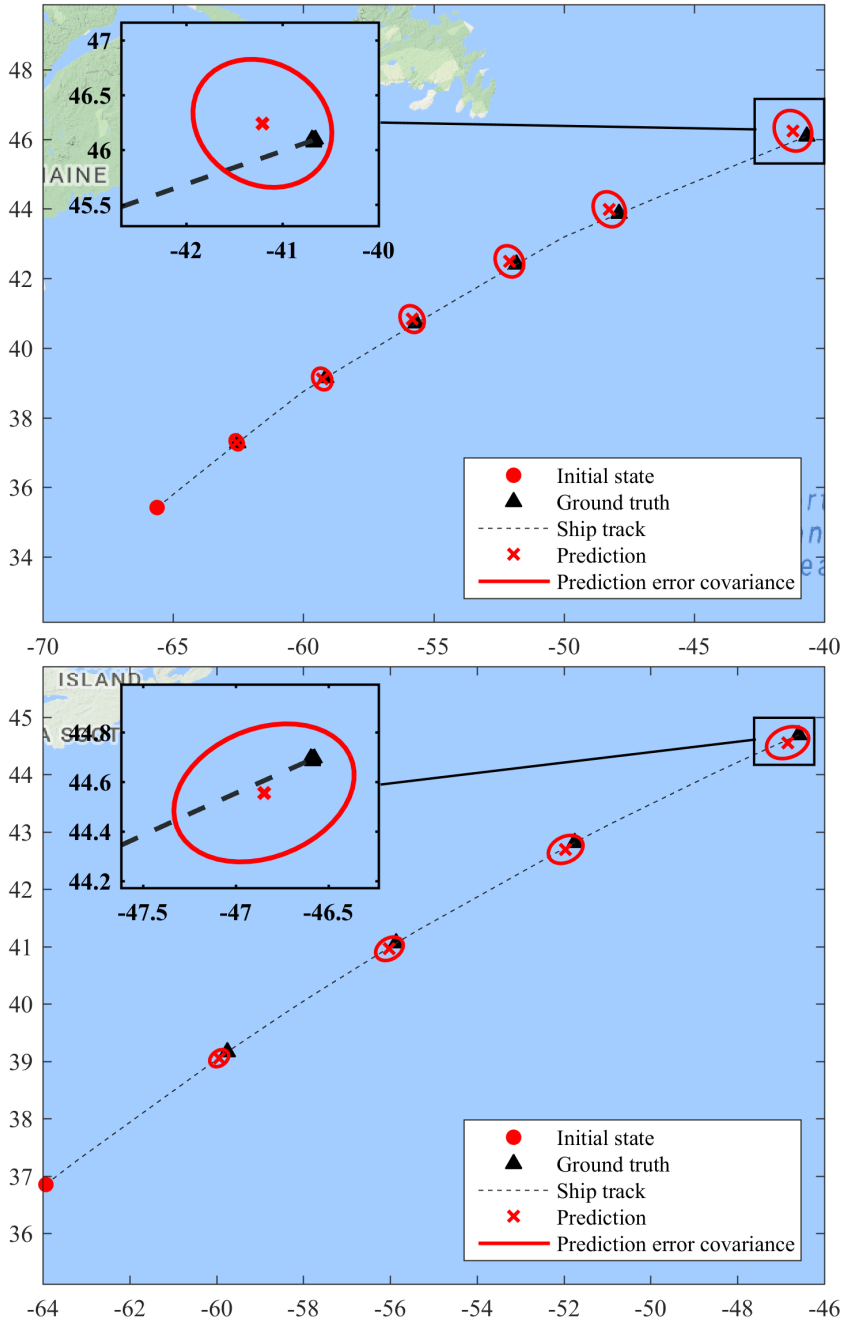

Figure 5: *Long-term association example with the proposed approach. Horizontal axis: longitude; vertical axis: latitude. Top panel: the "Hoegh Shanghai" container ship (MMSI* 258758000*) off the coast of Nova Scotia and the related position and error covariance after* $\approx$ 10, 20, 30, 40, 50 *and* 72 *hours from the initial state. Bottom panel: the "Mol Gratitude" container ship (MMSI* 477462400*) off the coast of Nova Scotia, with predictions at every* $\approx$ 12 *hours after the initial state. The last prediction is* $\approx$ 48 *hours after the initial state.*

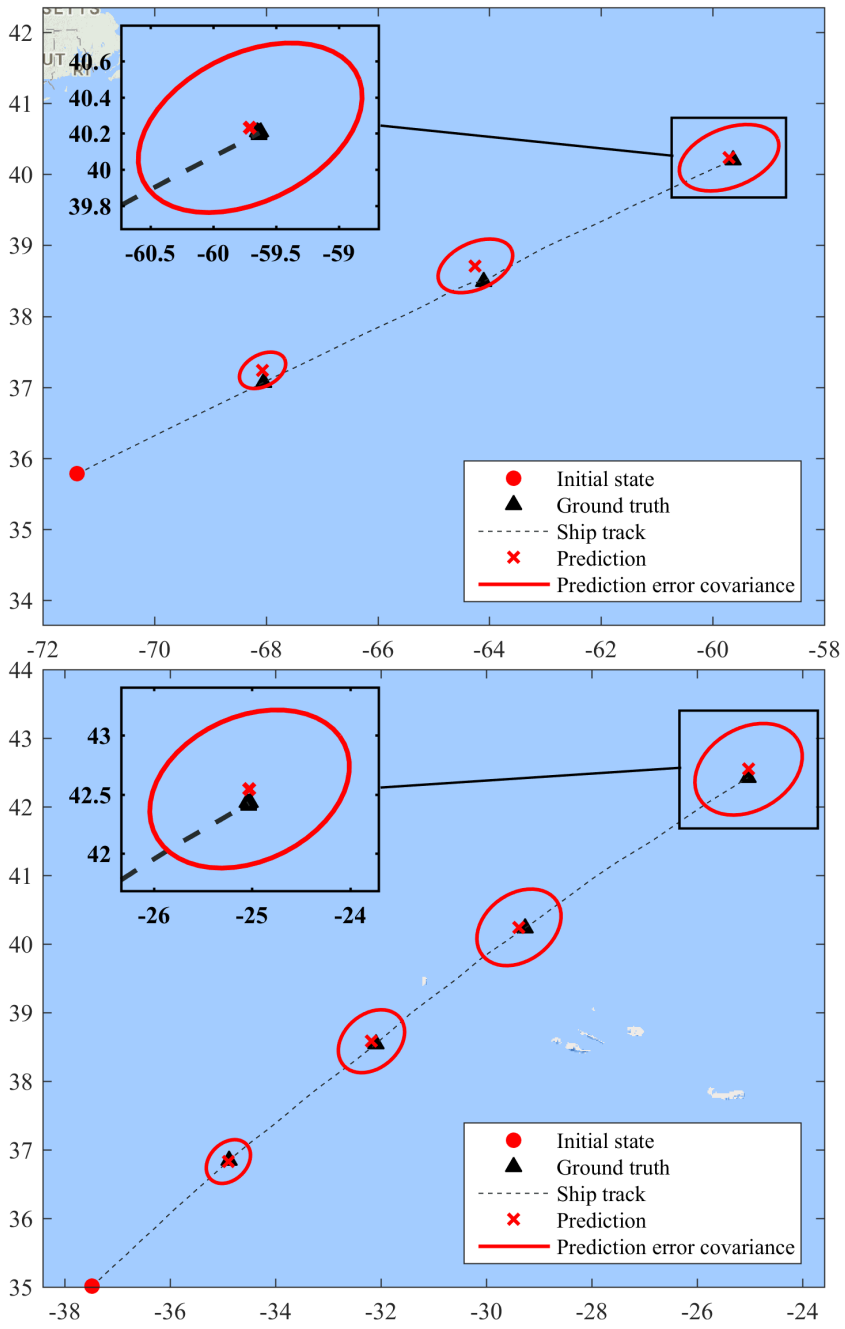

Figure 6: *Long-term association example with the proposed approach. Horizontal axis: longitude; vertical axis: latitude. Top panel: the "Eurasian Highway" vehicles carrier (MMSI* 432839000*) off the coast of Massachusetts and the related position and error covariance after* $\approx$ 10, 20 *and* 33 *hours from the initial state. Bottom panel: the "Vega Omikron" container ship (MMSI* 636092662*) in the North Atlantic Ocean, with predictions at every* $\approx$ 10 *hours after the initial state. The last prediction is* $\approx$ 45 *hours after the initial state.*

Table 1: *Estimated values of the OU process parameters for the ship tracks of the Canada data set considered in the experimental analysis.*

		$\boldsymbol{v}$		$\boldsymbol{\gamma}$		$\boldsymbol{\sigma}$	
		v_x	v_y	γ_x	γ_y	σ_x	σ_y
Fig. 3	top	-6.38	-4.23	$8.0 \cdot 10^{-4}$	$2.5 \cdot 10^{-3}$	$7.0 \cdot 10^{-3}$	$1.1 \cdot 10^{-2}$
	bottom	6.24	2.14	$4.0 \cdot 10^{-4}$	$6.1 \cdot 10^{-3}$	$3.5 \cdot 10^{-3}$	$8.6 \cdot 10^{-3}$
Fig. 4	top	8.78	4.58	$5.0 \cdot 10^{-4}$	$2.7 \cdot 10^{-3}$	$9.3 \cdot 10^{-3}$	$2.3 \cdot 10^{-2}$
	bottom	-7.98	-4.94	$1.1 \cdot 10^{-3}$	$8.0 \cdot 10^{-4}$	$1.5 \cdot 10^{-2}$	$1.7 \cdot 10^{-2}$
Fig. 5	top	8.03	4.68	$1.4 \cdot 10^{-3}$	$1.9 \cdot 10^{-3}$	$3.1 \cdot 10^{-2}$	$5.0 \cdot 10^{-2}$
	bottom	8.27	4.91	$1.4 \cdot 10^{-3}$	$2.5 \cdot 10^{-3}$	$4.7 \cdot 10^{-2}$	$5.7 \cdot 10^{-2}$
Fig. 6	top	8.67	4.17	$1.5 \cdot 10^{-4}$	$7.1 \cdot 10^{-4}$	$1.2 \cdot 10^{-2}$	$3.2 \cdot 10^{-2}$
	bottom	6.59	5.12	$3.7 \cdot 10^{-4}$	$5.0 \cdot 10^{-4}$	$1.7 \cdot 10^{-2}$	$1.7 \cdot 10^{-2}$

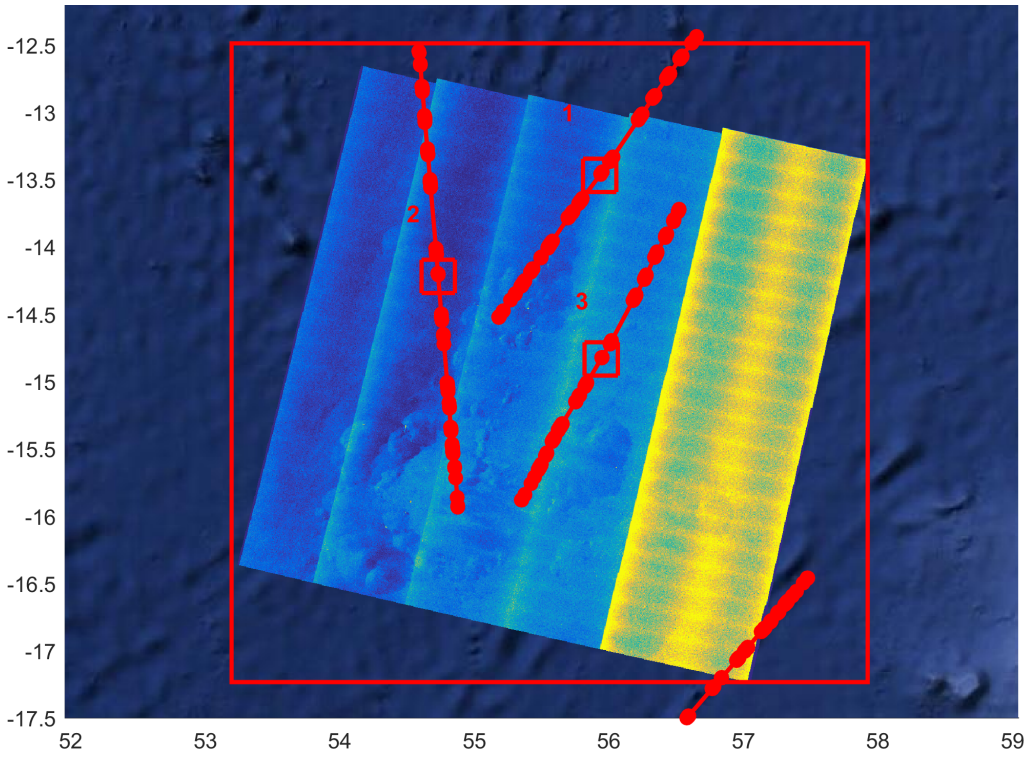

Figure 7: *SAR image used in the experimental analysis with AIS trajectories overlaid, which have been recorded in the area of the acquisition 6 hours prior and posterior to the acquisition time. Red circles denote the AIS contacts. The three red squares are centered in the positions of the vessels detected in the SAR image. A fourth AIS trajectory yields no association with any SAR detection, since the acquisition time does not result in the vessel being in the SAR frame of detection. Horizontal axis: longitude; vertical axis: latitude. Produced from ESA remote sensing data.*

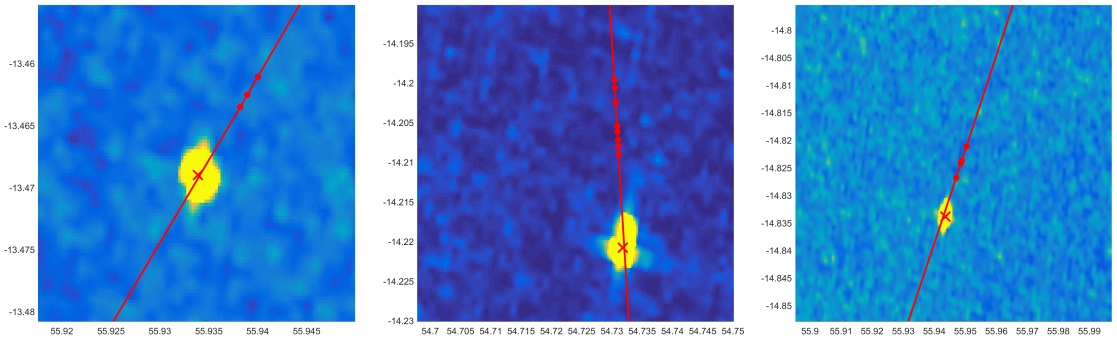

(a) Vessel 1 (b) Vessel 2 (c) Vessel 3

Figure 8: *SAR images of the three cargo ships used in the experimental analysis, matched with the corresponding AIS trajectories, overlaid in red. The category of the ship has been inferred from the AIS information. Red crosses denote the SAR detection, which is shown to be aligned with the corresponding AIS track in all the three cases. Horizontal axes: longitude; vertical axes: latitude. Produced from ESA remote sensing data.*

A qualitative analysis is performed first, and then the performance is assessed in terms of a performance metric, the GV (introduced in Section 4), as function of the prediction time.

This time, the test data set is made up by a SAR image acquired by Sentinel-1A on the 31st of May, 2016 off the coast of Madagascar, and by the S-AIS data collected the same day in the same region and stored in CMRE's historical AIS database. The data set is also shown in Figure 7, with spatio-temporally compatible AIS tracks overlaid in red. As it is shown by the closeups in Figure 8, three vessels can be detected by a simple visual inspection of the SAR image.

Figure 9 shows the SAR image at several zoom levels with overlaid the prediction based on the OU model and starting from an initial AIS state which was broadcast approximately 9 hours before the acquisition of the SAR image. The red ellipse is the prediction error covariance that one would get with the use of the NCV model, in place of the OU; it is unrealistically large, being even larger than the entire footprint of the SAR image, and it is shown only as a baseline reference. Conversely, the OU prediction error covariance is much more constrained around the SAR detection, and encompasses a single detection; in other words, with the OU model, there is no ambiguity in the association of the SAR detection with the corresponding AIS track.

Finally, in Figure 10, the evolution of the GV is reported as a function of the time, evaluated for the three detections in the dataset (Figure 8) and for the OU and NCV model [6, 8]; two versions of this latter model have been considered, which have two different prediction error scaling laws (proportionally to t^3 and t^4). The three different

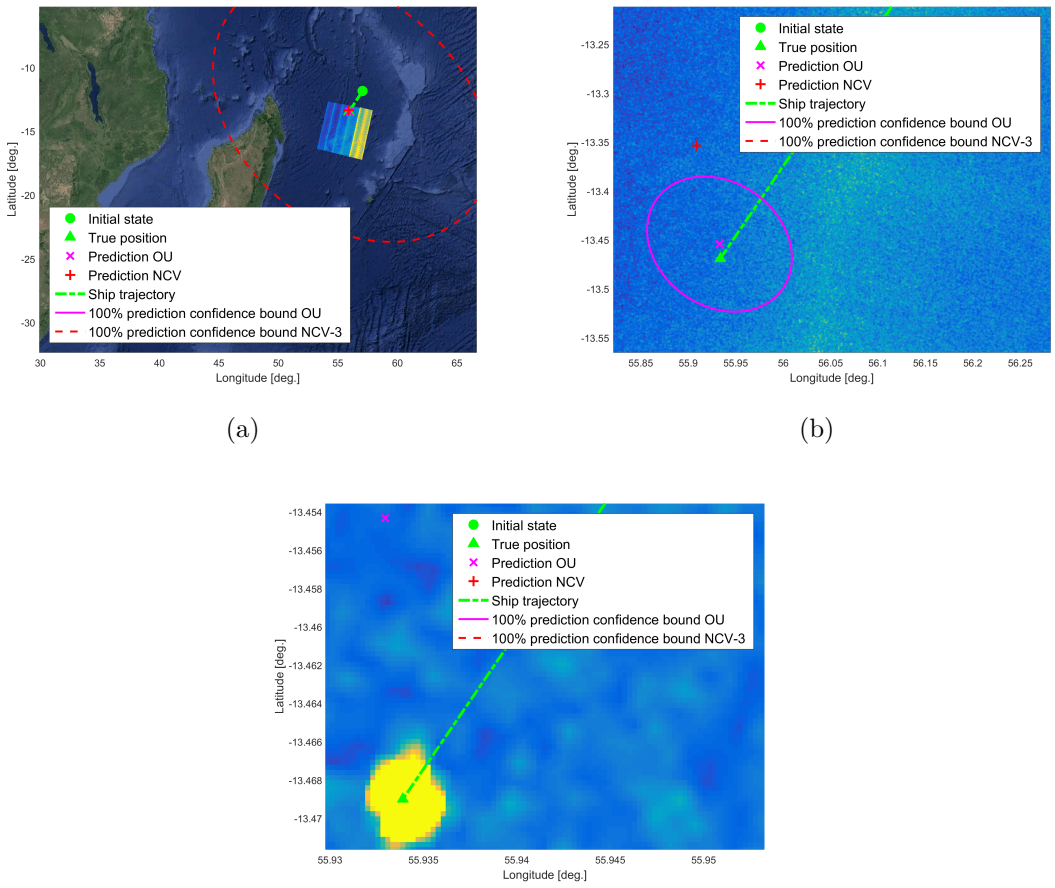

Figure 9: *SAR detection 1: (a) Overview; (b) and (c) Close-ups. The OU estimation of the vessel position (magenta cross) almost overlaps the true AIS position (green triangle), whereas NCV provides an estimation (red cross), which is several kilometers off the true position. Furthermore, the related 100%-confidence prediction covariance ellipses (plotted in red, NCV, and magenta, OU) are very different in size. Indeed, the OU size is considerably smaller than that of NCV. The AIS ship trajectory is depicted with green dashed line. Horizontal axis: longitude; vertical axis: latitude. Produced from ESA remote sensing data.*

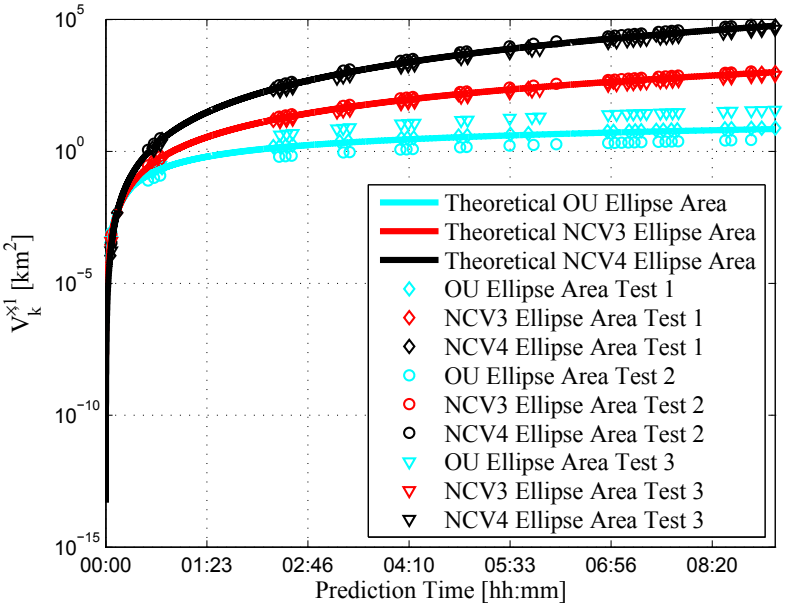

Figure 10: *Ellipse volumes over prediction time fixing $\gamma = 1$ and theoretical curves using average model parameters per ship category for the two NCV models and the OU model.*

markers define the measured volumes for the three vessels. The three colors indicate the three compared prediction models (i.e. OU in cyan, NCV3 in red, and NCV4 in black). The solid lines are instead obtained using the theoretical models [8] calculating the volumes for the three long-term prediction models. The advantage of using the OU model is that it leads to a significant reduction of the GV and, thus, a global reduction of ambiguity with respect to the NCV models. Such benefits become more significant for longer prediction times.

6.3 Canada data set: waypoint detection

The final use cases demonstrates the change detector, described in Section 5.1, at work. The data that has been used is once again taken from the Canada data set. Figures 11 and 12 depict two applications of the change detection procedure to two different tracks. The left-hand side panels show the ship trajectories, with a black triangle denoting the first data sample of the track. The red circles show the positions of the detected changes in the long-run mean parameter. In the right-hand side, from top to bottom, the instantaneous values of the Cartesian components of the velocity are shown over time, along x and y, after which the instantaneous speed and track orientation over time are reported, respectively; dots denote the instantaneous values, solid lines their long-run mean counterparts and circles the change detections.

Although it is not immediately clear how to properly assess the *quality* of the change detector's output by a simple visual inspection, the plots in the right panels of each figure show that the procedure is able to achieve what appears to be a reasonable result in term of detection of abrupt changes and estimation of the long-run mean velocity regimes.

This operation can be repeated for every ship track in a given region of interest, obtaining a set of change detections with corresponding long-run mean velocity values before and after the change. With regular traffic such as that shown in shown in Figure 1, the change detections are expected to *condense* around common waypoint regions which can be identified and connected in order to build a graph model for the maritime traffic. The theoretical and empirical tools to achieve such a result are beyond the scope of this document and are instead document in a companion report—Part II.

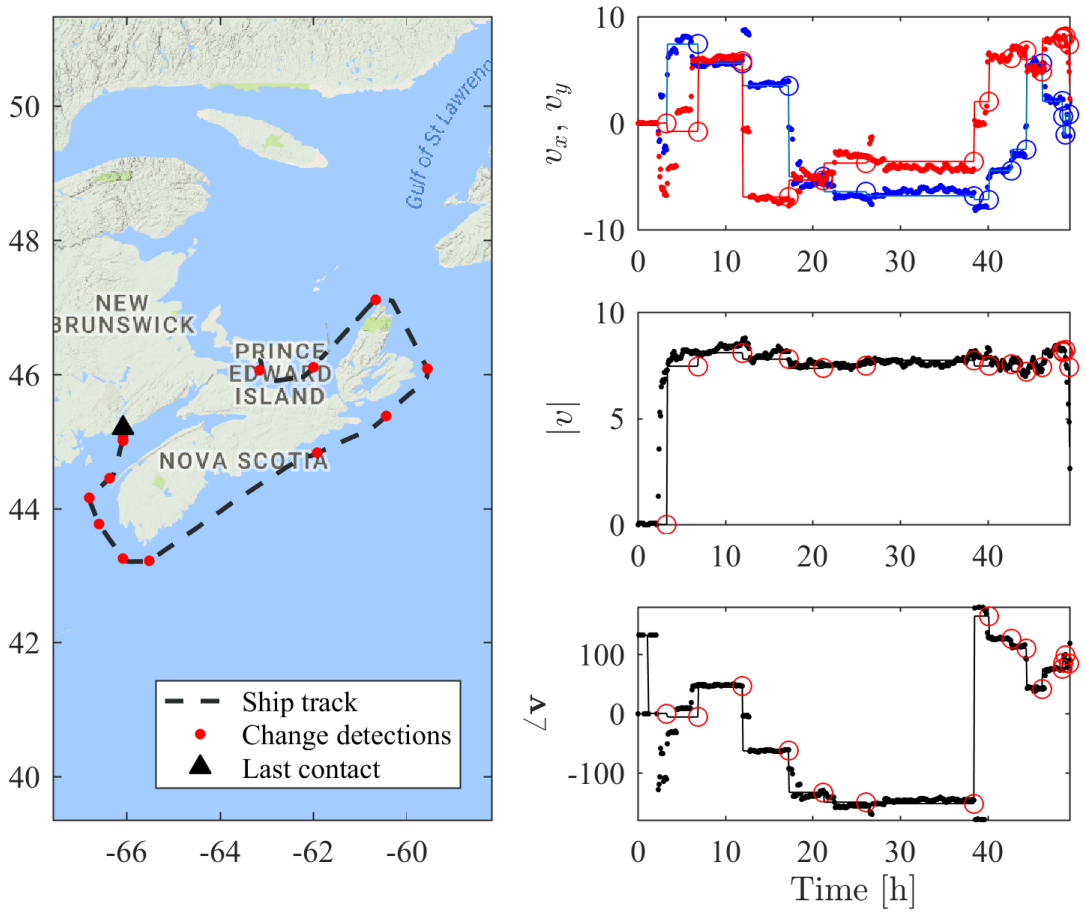

Figure 11: *Example of the change detection procedure applied to a single track, made up by the positions broadcast by the "Acadian" oil/chemical tanker (MMSI* 316012950*). The left-hand side panel shows the selected track, with the horizontal and vertical axes reporting longitude and latitude, respectively. The black triangle denotes the last data sample of the track and therefore shows the motion direction. The red circles show the detected changes in the parameter. Right-hand side, from top to bottom: instantaneous value of the Cartesian components of the velocity over time, along x and y, respectively, and instantaneous track orientation; dots denote the instantaneous values, solid lines the value of the parameter, and circles the change detections.*

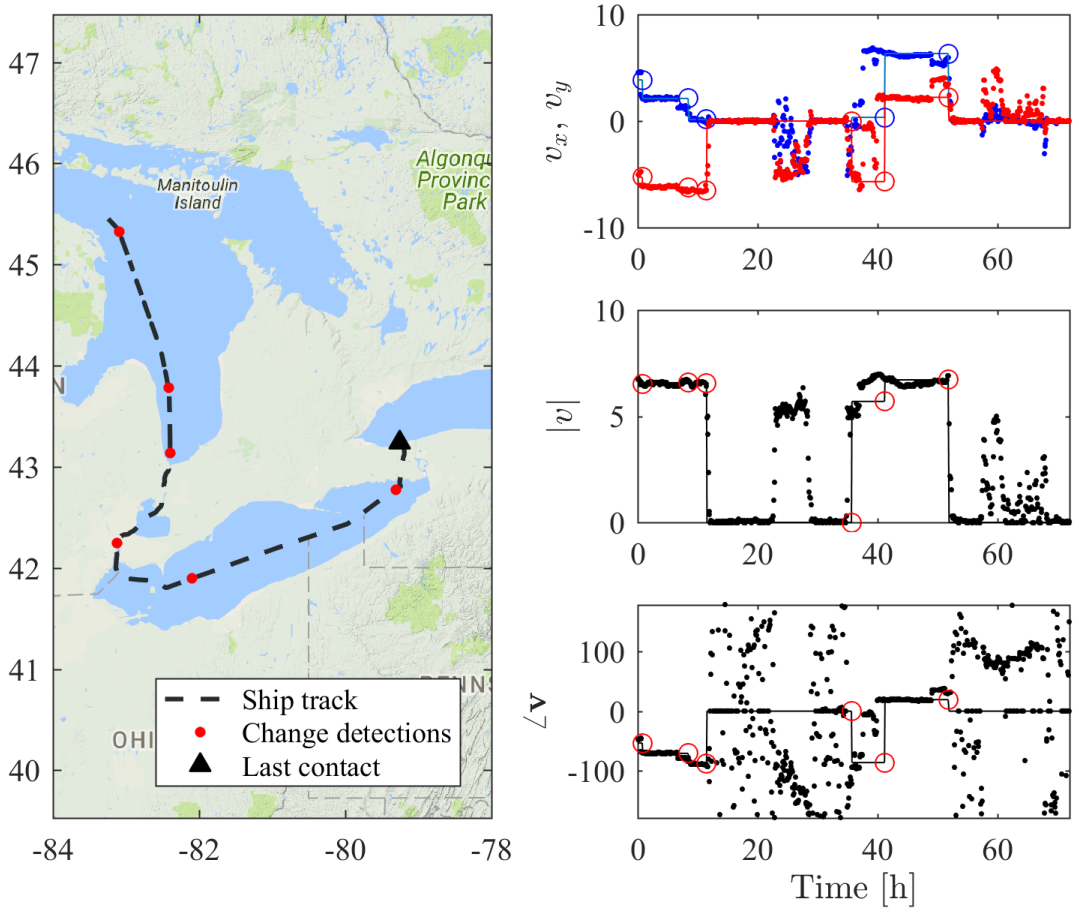

Figure 12: *Example of the change detection procedure applied to a single track, made up by the positions broadcast by the "Arneborg" cargo vessel (MMSI* 246556000*). The left-hand side panel shows the selected track, with the horizontal and vertical axes reporting longitude and latitude, respectively. The black triangle denotes the last data sample of the track and therefore shows the motion direction. The red circles show the detected changes in the parameter. Right-hand side, from top to bottom: instantaneous value of the Cartesian components of the velocity over time, along x and y, respectively, and instantaneous track orientation; dots denote the instantaneous values, solid lines the value of the parameter, and circles the change detections. The careful reader will notice a missed change detection between* 20 *and* 40 *hours. This behavior can be ascribed to the noisy velocity angle. The noise in the instantaneous velocity angle is an artifact resulting from the challenges in computing the angle of a vector whose magnitude is very close to zero.*

7 Conclusion and future work

The idea to discover spatio-temporal patterns from moving object data is not new, and indeed various and diverse approaches can be found in literature dealing with the synthesis of spatio-temporal moving object data into concise patterns. These patterns can be seen as abstract and synthetic representations of aggregates of many, similar individual trajectories of objects in motion. Such representations do not only provide insights on the underlying data structures, but also open up to a number of interesting opportunities such as classification, anomaly detection, categorizing activities, and prediction of future behaviors.

A well-known feature of global maritime traffic is that the majority of it is very regular: ships, especially those involved in the transportation of goods, often if not always seek to optimize fuel consumption, and therefore will naturally follow the most convenient path allowed by international regulations and traffic separation schemata. Nonetheless, a technique to efficiently process massive amounts of spatio-temporal traffic data to reveal the underlying network structure, in the form of a graph or a graphical model, has not yet been universally identified.

This report is built around the intuition that there is a feedback loop in a ship's motion and therefore the velocity of a vessel is not completely random. It has documented the modeling of the motion of a non-maneuvering ship through a stochastic mean-reverting process that represents its velocity, from the mathematical formalization to the derivation of a Bayesian-optimal prediction procedure that can be used for long-term prediction and association of measurements from heterogeneous and highly asynchronous sensors. Suitable procedures for the estimation of the parameters of the stochastic process and for gating heterogeneous and asynchronous data have been presented as well. Then, the model has been extended to the case of ship waypoint navigation, and a statistical change detection procedure has been developed to identify the time instants of change and, correspondingly, the navigational waypoints. Finally, some selected experimental results have been reported, in order to demonstrate the relevance of the modeling to real-world applications, and real-world data.

Altogether, this report has laid the theoretical background to enable the development of knowledge discovery techniques in a probabilistic framework, which is documented in the companion report—Part II.

References

[1] Del Pozo, F., Dymock, A., Feldt, L., Hebrard, P., and di Monteforte, F. S. (2010), Maritime surveillance in support of CSDP, Vol. 26.

[2] Cimino, G., Arcieri, G., Horn, S., and Bryan, K. (2014), Sensor data management to achieve information superiority in Maritime Situational Awareness, (Technical Report CMRE-FR-2014-017, NATO UNCLASSIFIED) NATO STO CMRE.

[3] Millefiori, L. M., Vivone, G., Braca, P., Cazzanti, L., and Bryan, K. (2016), Maritime Situational Awareness use cases enabled by space-borne sensors, In *Proc. of the SCI-283 "Considerations for Space and Space-Enabled Capabilities in NATO Coalition Operations" Meeting*.

[4] Ristic, B., Scala, B. L., Morelande, M., and Gordon, N. (2008), Statistical analysis of motion patterns in AIS Data: Anomaly detection and motion prediction, In *2008 11th International Conference on Information Fusion (FUSION)*, pp. 1–7.

[5] Pallotta, G., Vespe, M., and Bryan, K. (2013), Vessel Pattern Knowledge Discovery from AIS Data: A Framework for Anomaly Detection and Route Prediction, *Entropy*, 15(12), 2218–2245.

[6] Rong Li, X. and Jilkov, V. (2003), Survey of maneuvering target tracking. Part I. Dynamic models, *IEEE Transactions on Aerospace and Electronic Systems*, 39(4), 1333–1364.

[7] Bar-Shalom, Y., Willett, P., and Tian, X. (2011), Tracking and Data Fusion: A Handbook of Algorithms, Storrs, CT: YBS Publishing.

[8] Millefiori, L. M., Braca, P., Bryan, K., and Willett, P. (2016), Modeling Vessel Kinematics using a Stochastic Mean-Reverting Process for Long-Term Prediction, *IEEE Transactions on Aerospace and Electronic Systems*, 52(5), 2313–2330.

[9] Stone, L. D., Barlow, C. A., and Corwin, T. L. (1999), Bayesian multiple target tracking, Artech House.

[10] Coraluppi, S. and Carthel, C. (2012), Stability and stationarity in target kinematic modeling, In *IEEE Aerospace Conference,*, pp. 1–8.

[11] Coraluppi, S. and Carthel, C. (2012), A hierarchical MHT approach to ESM-radar fusion, In *Information Fusion (FUSION), 2012 15th International Conference on*, pp. 677–683.

[12] Millefiori, L. M., Pallotta, G., Braca, P., Horn, S., and Bryan, K. (2015), Validation of the Ornstein-Uhlenbeck route propagation model in the Mediterranean Sea, In *OCEANS 2015 - Genova*, IEEE.

[13] Maybury, D. W. (2017), Ship propagation as a harmonically bound particle: Using the Kramers equation for vessel traffic data, (DRDC-RDDC-2017-R045) Defence Research and Development Canada – Centre for Operational Research and Analysis.

[14] Langevin, P. (1908), Sur la théorie du mouvement brownien, *C. R. Acad. Sci. (Paris)*, pp. 530–533.

[15] Gillespie, D. (1996), Exact numerical simulation of the Ornstein-Uhlenbeck process and its integral, *Phys. Rev. E*, 54(2), 2084–2091.

[16] Øksendal, B. (2003), Stochastic differential equations, Springer.

[17] Uhlenbeck, G. E. and Ornstein, L. S. (1930), On the theory of Brownian motion, *Phys. Rev.*, 36, 823–841.

[18] Barndorff-Nielsen, O. E. and Shephard, N. (2003), Integrated OU processes and non-Gaussian OU-based stochastic volatility models, *Scand. J. Statist.*, 30(2), 277–295.

[19] Gardiner, C. W. et al. (1985), Handbook of stochastic methods, Vol. 4, Springer Berlin.

[20] Valdivieso, L., Schoutens, W., and Tuerlinckx, F. (2009), Maximum likelihood estimation in processes of Ornstein-Uhlenbeck type, *Statistical Inference for Stochastic Processes*, 12(1), 1–19.

[21] Franco, J. C. G. (2003), Maximum likelihood estimation of mean reverting processes, *Real Options Practice*.

[22] Millefiori, L. M., Braca, P., and Willett, P. (2016), Consistent Estimation of Randomly Sampled Ornstein-Uhlenbeck Process Long-Run Mean for Long-Term Target State Prediction, *IEEE Signal Processing Letters*, 23(11), 1562–1566.

[23] Challa, S., Morelande, M. R., Mušicki, D., and Evans, R. J. (2011), Fundamentals of object tracking, Cambridge University Press.

[24] Basseville, M. and Nikiforov, I. V. (1993), Detection of Abrupt Changes: Theory and Application, Englewood Cliffs, N.J: Prentice-Hall.

[25] Page, E. (1954), Continuous inspection schemes, *Biometrika*, 41, 100–115.

[26] Millefiori, L. M., Braca, P., and Arcieri, G. (2017), Scalable distributed change detection and its application to maritime traffic, In *2017 IEEE International Conference on Big Data (Big Data)*, IEEE.

Acronyms

AIS Automatic Identification System

ARL Average Run Length

CMRE Centre for Maritime Research and Experimentation

CRLB Cramér-Rao Lower Bound

CUSUM Cumulative Sum

DRDC Defence Research and Development Canada

ESA European Space Agency

GLR Generalized Likelihood Ratio

GPS Global Positioning System

GV Gate Volume

IOU Integrated Ornstein-Uhlenbeck

LS Least Squares

ML Maximum Likelihood

MMSI Maritime Mobile Service Identifier

MSA Maritime Situational Awareness

NCV Nearly Constant Velocity

OU Ornstein-Uhlenbeck

PDF Probability Density Function

RCN Royal Canadian Navy

RDD Resilient Distributed Dataset

S-AIS Satellite AIS

SAR Synthetic Aperture Radar

SDE stochastic differential equation

SME Sample Mean Estimator

UTM Universal Transverse Mercator

DOCUMENT CONTROL DATA

*Security markings for the title, authors, abstract and keywords must be entered when the document is sensitive

1. ORIGINATOR (Name and address of the organization preparing the document. A DRDC Centre sponsoring a contractor's report, or a tasking agency, is entered in Section 8.)

DRDC – Centre for Operational Research and Analysis
Carling Campus, 60 Moodie Drive, building 7S.2, Ottawa, ON K1A 0K2, Canada

2a. SECURITY MARKING (Overall security marking of the document, including supplemental markings if applicable.)

CAN UNCLASSIFIED

2b. CONTROLLED GOODS

NON-CONTROLLED GOODS
DMC A

3. TITLE (The document title and sub-title as indicated on the title page.)

Pattern of life model parameterization for exploitation in Command and Control systems: Methodology report part I: Target motion model and formalization

4. AUTHORS (Last name, followed by initials – ranks, titles, etc. not to be used. Use semi-colon as delimiter)

Millefiori, L. M.; Braca, P.; Horn, S.

5. DATE OF PUBLICATION (Month and year of publication of document.)	6a. NO. OF PAGES (Total pages, including Annexes, excluding DCD, covering and verso pages.)	6b. NO. OF REFS (Total cited in document.)
September 2019	41	26

7. DOCUMENT CATEGORY (e.g., Scientific Report, Contract Report, Scientific Letter)

Scientific Report

8. SPONSORING CENTRE (The name and address of the department project or laboratory sponsoring the research and development.)

DRDC – Centre for Operational Research and Analysis
Carling Campus, 60 Moodie Drive, building 7S.2, Ottawa, ON K1A 0K2, Canada

9a. PROJECT OR GRANT NO. (If appropriate, the applicable research and development project or grant number under which the document was written. Please specify whether project or grant.)	9b. CONTRACT NO. (If appropriate, the applicable contract number under which the document was written.)
01da	

10a. DRDC DOCUMENT NUMBER	10b. OTHER DOCUMENT NO(s). (Any other numbers which may be assigned this document either by the originator or by the sponsor.)
DRDC-RDDC-2019-R058	

11a. FUTURE DISTRIBUTION WITHIN CANADA (Approval for further dissemination of the document. Security classification must also be considered.)

Public release

11b. FUTURE DISTRIBUTION OUTSIDE CANADA (Approval for further dissemination of the document. Security classification must also be considered.)

Public release

12. KEYWORDS, DESCRIPTORS or IDENTIFIERS (Use semi-colon as a delimiter.)

pattern of life; Machine Learning; Situational Awareness

13. ABSTRACT/RÉSUMÉ (When available in the document, the French version of the abstract must be included here.)

Extracting valuable information from large spatio-temporal datasets requires innovative approaches that can efficiently deal with large amounts of data and, at the same time, effectively reveal the underlying structure of the data, in order to provide useful information to the decision making process.

Innovative knowledge discovery techniques have been developed which use a stochas-tic mean-reverting modeling of the ships motion to reveal the underlying graphical structure of maritime traffic. The generated knowledge enables numerous possibil-ities, from graph-based multi-edge prediction to anomaly detection techniques, to ship routing optimization. Altogether, the topics covered in this report represent the theoretical framework that is required for the development of knowledge discovery techniques able to reveal the underlying graph structure of maritime traffic, which are documented in the companion report—Part II.

This report—Part I—documents the formalization of the ship motion model, moti-vating its use over other conventional models. Procedures to estimate the process parameters are provided and its use for long-term prediction and data association is investigated. The main limitation of this model, its applicability to non-maneuvering targets only, is also overcome by formalizing an augmented version of the model that fits the case of a vessel navigating by waypoints. Real-world data sets are used to show the potential of the developed techniques in cases of practical relevance.

This work was done within the DRDC-CMRE collaborative research activity “Pattern of life model parameterization for exploitation in Command and Control systems" under the DRDC Project 01da on Next Generation Naval Command and Control Systems.

L’extraction de l’information précieuse à partir de grands ensembles de données spatio-temporelles nécessite des approches novatrices en mesure de traiter efficacement un grand volume d’information tout en révélant la structure sous-jacente des données. Elle est ainsi capable de fournir des renseignements utiles au processus décisionnel.

On a mis au point des techniques novatrices de découverte des connaissances à l’aide d’une modélisation stochastique du mouvement des navires par retour à la moyenne en vue de révéler la structure graphique sous-jacente du trafic maritime. Les connaissances générées offrent de nombreuses possibilités, allant de la prédiction multibord graphique aux techniques de détection d’anomalies, en passant par l’optimisation des routes des navires. Regroupés, les sujets abordés dans le présent rapport représentent le cadre théorique nécessaire à l’élaboration de techniques de découverte des connaissances capables de révéler la structure graphique sous-jacente du trafic maritime, qui sont documentées dans le rapport complémentaire - Partie II.

Le présent rapport, Partie I, documente la formalisation du modèle de mouvement du navire et promeut l’emploi de ce dernier plutôt que des autres modèles conventionnels. En outre, il comprend des procédures d’estimation des paramètres du processus et on y étudie l’information sur l’exécution de ce processus dans le cadre de la prévision à long terme et de l’association de données. La principale limite de ce modèle, à savoir son applicabilité à des cibles sans manoeuvres seulement, est surmontée par la formalisation d’une version améliorée adaptée au cas d’un navire naviguant à l’aide de points de cheminement. On utilise des ensembles de données en situation réelle afin de démontrer le potentiel des techniques élaborées dans des cas d’intérêt pratique.

On a réalisé ce travail dans le cadre de l’activité de recherche concertée de RDDC CREM «paramétrage du modèle du mode de vie aux fins d’exploitation dans les systèmes de commandement et de contrôle » du projet 01da de RDDC sur les systèmes de commandement et de contrôle navals de prochaine génération.